D. Buscombe, Marda Science LLC, contracted to U.S. Geological Survey Pacific Coastal & Marine Science Center, Santa Cruz, CA, USA. dbuscombe@contractor.usgs.gov

J.A. Warrick; U.S. Geological Survey Pacific Coastal & Marine Science Center, Santa Cruz, CA, USA

A. Ritchie; U.S. Geological Survey Pacific Coastal & Marine Science Center, Santa Cruz, CA, USA

A. East; U.S. Geological Survey Pacific Coastal & Marine Science Center, Santa Cruz, CA, USA

M. McHenry; Lower Elwha Klallam Tribe, WA, USA

R. McCoy; Lower Elwha Klallam Tribe, WA, USA

A. Foxgrover; U.S. Geological Survey Pacific Coastal & Marine Science Center, Santa Cruz, CA, USA

E. Wohl; Colorado State University, Fort Collins, CO, USA

Remote sensing large-wood storage downstream of reservoirs during and after dam removal: Elwha River, Washington, USA

Buscombe, D.[1], J.A. Warrick[2], A. Ritchie[2], A. East[2], M. McHenry[3], R. McCoy[3], A. Foxgrover[2], and E. Wohl[4]

[1]Marda Science LLC, contracted to U.S. Geological Survey Pacific Coastal & Marine Science Center, Santa Cruz, CA, USA; [2]U.S. Geological Survey Pacific Coastal & Marine Science Center, Santa Cruz, CA, USA; [3]Lower Elwha Klallam Tribe, WA, USA; [4]Colorado State University, Fort Collins, CO, USA

Abstract

Large wood is an integral part of many rivers, often defining river-corridor morphology and habitat, but its occurrence, magnitude, and evolution in a river system are much less well understood than the sedimentary and hydraulic components, and due to methodological limitations, have seldom previously been mapped in substantial detail. We present a new method for this, representing a substantial advance in automated deep-learning-based image segmentation. From these maps, we measured large wood and sediment deposits from high-resolution orthoimages to explore the dynamics of large wood in two reaches of the Elwha River, Washington, USA, between 2012 and 2017 as it adjusted to upstream dam removals. The dataset consists of a time series of orthoimages (12.5-cm resolution) constructed using Structure-from-Motion photogrammetry on imagery from 14 aerial surveys. Model training was optimized to yield maximum accuracy for estimated wood areas, compared to manually digitized wood, therefore model development and intended application were coupled. These fully reproducible methods and model resulted in a maximum of 15% error between observed and estimated total wood areas and wood deposit size-distributions over the full spatio-temporal extent of the data. Areal extent of wood in the channel margin approximately doubled in the years following dam removal, with greatest increases in large wood in wider, lower-gradient sections. Large-wood deposition increased between the start of dam removal (2011) and winter 2013, then plateaued. Sediment bars continued to grow up until 2016/17, assisted by a partially static wood framework deposited predominantly during the period up to winter 2013.

Plain language summary

We measure the large wood in the Elwha River, Washington, USA, during and after dam removal. The presence of two dams had previously limited the movement of sediment and wood through the system. The removal of those dams liberated large amounts of sediment and wood from the former reservoir bottoms, which traveled downstream and deposited in the river channel. We develop an Artificial Intelligence (AI) model to measure all wood and sediment in the Elwha River corridor downstream of the two former dams, from a time-series of high-resolution imagery collected from aircraft. These measurements, accurate to within 15% of true values, provide a unique opportunity to understand how large wood occurs and behaves over multiple years and tens of kilometers. We found that the deposition of large wood on bars was coincident with and promoted the growth of sediment bars. The AI model we made could be powerful enough to find large wood in other places and images for similar purposes. Our datasets and models are made available to stimulate further studies of changes in river form resulting from interactions between water flow, wood, sediment, and vegetation.

1. Introduction

1.1. Large wood in rivers

The occurrence and movement of large wood (downed, dead pieces greater than 10 cm in diameter and 1 m long; Wohl et al., 2019a) can significantly influence the evolution of river ecosystems through bio-geomorphic feedbacks (Ruiz-Villanueva et al., 2016; Wohl et al., 2019b). In recent decades, a growing literature has documented the beneficial effects of large wood in rivers, revealing the importance of the roles that large wood plays in creating in-stream habitats (Frissell et al., 1986; Fetherston et al., 1995; Abbe and Montgomery, 1996), longitudinal and lateral (i.e., river-floodplain) connectivity (Beechie et al., 2006; Wohl et al., 2019a; Swanson et al., 2021), channel braiding and avulsion (Wohl et al., 2019a; Swanson et al., 2021), bio-geomorphic interactions (Wohl et al., 2019b), and nutrient cycling (Collins et al., 2012), among others, summarized by Wohl et al. (2017). In addition, the importance of large wood in river restoration, dam removal, fisheries, fish passage, spawning and rearing habitat,

among other important aspects of applied river science, have been the subject of review by Gurnell et al. (2002), Abbe et al. (2003), Nagayama and Nakamura (2010), Wohl (2017, 2020), Wohl et al., (2019), and Swanson et al., (2021).

Wohl et al. (2019a) conceptualized the influence of interactions among water, sediment, and wood on river corridors. Emergent properties of these interactions result in a physical habitat "template" that includes the amount, diversity, and quality of available physical habitats, the connectivity of the river channel with its floodplain, dissolved nutrient availability, and water quality (Collins et al., 2012). In settings such as the U.S. Pacific Northwest, the physical habitat template is strongly influenced by the presence of mobile and stored wood (e.g., Fetherston et al., 1995; Abbe and Montgomery, 1996; Beechie et al., 2006; Scott and Wohl 2018).

Depending on context, wood may be stored within the active channel for a varying amount of time, from less than 1 year to more than 10,000 years (e.g., Nanson et al. 1995; Wohl, 2017). Stored wood influences geomorphic processes such as sediment transport, deposition, and storage, and the formation of morphologies such as steps, pools, bars, and secondary channels (e.g., Abbe and Montgomery, 1996; Wohl et al., 2017; Grabowski and Wohl, 2021). As channel complexity increases, we expect more wood deposition, and vice versa, with hypothesized feedback processes involved (Wohl et al., 2017). At the scale of reaches, large wood is thought to suppress sediment transport and promote sediment deposition through increased hydraulic roughness (Davidson and Eaton, 2013; Wohl, 2017) and to promote hydraulic and topographic complexity, which can promote the storage of organic matter (Pfeiffer and Wohl, 2018). For example, persistent jams of large wood are understood to trap sediment to the point that they have even been responsible for the conversion of bedrock reaches to alluvial reaches (Montgomery et al., 1996; Massong and Montgomery, 2000).

Humans have extensively modified wood recruitment (the process of wood entering an active channel or floodplain), and the abundance, sizes, mobility, and spatial distributions in river channels during the modern industrial and post-industrial ages. Large wood in river channels has been a harvested resource of opportunity or removed by humans because of concerns about flooding, fish passage, and/or riverbank erosion

(Wohl, 2019; Moulin and Piegay, 2004; Abbe and Montgomery, 1996; Comiti et al., 2016). Additionally, the sources of wood from old-growth forests have been eliminated from many watersheds from logging, and dam construction across rivers worldwide may reduce wood transport downstream because of wood impoundment and removal and hydromodifications to downstream flow regimes (Comiti et al., 2008; Wohl, 2011). This widespread loss of wood has led to incidences of channel incision, including the transformation of alluvial channels into bedrock channels (Stock et al., 2005; Schanz et al., 2018). The loss of longitudinal connectivity with respect to large wood has also created detrimental changes in coastal, nearshore, and even deep-sea environments (Wohl and Iskin, 2021).

Because of the general reduction of wood in many rivers over time, restoration efforts often include an enhancement of wood abundance to increase channel complexity and improve habitat (Warren and Kraft, 2008; Roni et al., 2015; Grabowski et al., 2019). Dam removal has the potential to enhance downstream wood and sediment storage, but studies of these changes – especially of wood – are rare (Major et al., 2017). In one prior study, large wood was documented to play a role in reservoir erosion and channel evolution after the Merrimack Village Dam was removed on the Souhegan River, New Hampshire (Pearson et al., 2011). McDowell and Hassan (2024) also reported on channel changes that resulted from the removal of an upstream culvert and subsequent large sediment pulse. Changes were found to be exacerbated by the presence of a logjam that formed when the culvert was removed.

Given the importance of large wood in river ecology, geomorphology, and hydrology, a better understanding of the physical, ecological, and engineering role of large wood will contribute to both better natural resource management and better hazard risk assessment and mitigation (Abbe and Brooks, 2011; Wohl et al., 2016). To achieve this, measurements of the size, abundance, persistence, and geomorphic setting of large wood are needed, over both large scales of time and distance within river corridors. These kinds of measurements, especially if paired with efforts by the large-wood research community toward standardization of methods and packaging of accessible software, will allow for comprehensive assessments of wood storage patterns and

persistence, which Wohl et al. (2017) and Swanson et al. (2021) identified as major knowledge gaps in riverine wood science. Such data might help better realize management objectives such as defining "target wood regimes" (Wohl et al., 2019a), which would help balance desired geomorphic and ecological characteristics with large-wood-related management and hazard-mitigation considerations for any given system. Additionally, repeatable measurements of large-wood abundance and distribution will inform efforts to quantitatively assess the role of wood in river form and functions (Wohl et al., 2019a; Wohl., 2020).

1.2. Remote-sensing approach to large-wood monitoring

Of particular interest to the studies of wood in riverine and coastal systems are repeatable methods that can be applied to measure wood and other channel components at large spatial scales and over long timescales. A viable alternative to field work to amass these measurements, especially at catchment scales, is the use of aerial remote sensing to quantify wood visible at the surface (Sendrowski and Wohl, 2021). One advantage of a remote-sensing approach is its potential to capture a synoptic measurement of all wood in a system at a single moment in time, including wood that may be relatively inaccessible by foot or vehicle. Given the decimeter-to-meter scale of some smaller wood accumulations, LiDAR or imagery with voxel or pixel spatial footprints much less than 1-m must typically be used. This precludes the use of most of the publicly available satellite imagery, which typically consists of pixels with a spatial footprint larger than 1 m, for quantifying wood accumulations of all sizes. Close-range cameras with an oblique vantage have been used for small sub-reach-scale studies of large-wood dynamics (e.g., Bertoldi et al., 2013), but this approach is limited in spatial extent. Aerial remote sensing of wood presence and transport in whole river corridors using LiDAR (e.g., Bertoldi et al., 2013; Atha and Dietrich, 2016; Kuiper et al., 2023), 3D point clouds from structure-from-motion (SfM) photogrammetry (e.g., Spreitzer et al., 2019), or nadir-perspective aerial imagery (orthoimagery, e.g., Haschenburger and Rice 2004; Smikrud and Prakash, 2006; Lassettre et al., 2008; Atha, 2014; Taminga et al., 2015; Kramer et al., 2017; Sanhueza et al., 2019; Tsunetaka et al., 2021; Iroumé et al.,

2023; Sendrowski et al., 2023) are all promising and relatively new means to investigate the spatiotemporal properties and longevity of wood storage at the scale of the river corridor over multiple years (Ruiz-Villanueva et al., 2016).

Imagery from a wide range of aerial platforms provide opportunities to observe and quantify large wood in river systems over a spectrum of spatial and temporal scales (Table 1). Prior measurements from imagery have generally used manual digitization of wood accumulations or manually supervised image-processing workflows, rather than fully automated means. Out of 14 prior studies, nine used entirely manual wood detection, and five used semi-automated image-processing methods for wood detection (Table 1). These methods require manual specification of parameters, image feature representations, and/or manual investigation of appropriate image features to extract and use for wood detection. One prior method, that of Sendrowski et al. (2023), used Deep Learning (DL) to automate the process of wood detection. In this work Sendrowski et al. (2023) showed that so-called 'binary' image-segmentation, whereby image pixels are classified as wood or not wood, could effectively be used within a supervised DL framework at a large scale and from high-resolution remotely sensed imagery. Manual work is also required for DL models, such as Sendrowski et al. (2023), specifically in the development of the data required for model training. But once trained to provide measurements at sufficient accuracy and verified that the model works well over the requisite spatial and temporal scale, no additional manual effort should be necessary. Development and validation of such models remains a challenge, but once completed, a trained model instance such as that of Sendrowski et al. (2023), when made available to other researchers, may transfer well to the task of recognizing similar large-wood deposits (e.g., tree species, dimensions) in similar imagery (e.g., pixel size) of other alluvial systems, which has been demonstrated of DL models in other similar contexts (Kentsch et al. 2020; Vandaele et al. 2021). A transferable model such as this may be deemed useful as-is, upon completion of a straightforward verification based on manual digitized measurements. Alternatively, a modest amount of fine-tuning of the model may be carried out based on new labeled data. Both contexts are referred to in the DL literature as Transfer Learning, an umbrella term of strategies designed to maximize the utility of trained model instances with minimal amounts of new labeled data, often

owing to the considerable effort required to train DL models from scratch, both in terms of large datasets required, and potentially significant model training time.

Repeated remote sensing of a study area for large-wood monitoring, consisting of spatially and temporally explicit analyses of a time series of imagery with identical spatial coverage, will facilitate measurements of wood presence, absence, and persistence for every pixel location in the dataset, which can be aggregated into larger spatial scales for subsequent analysis. Such measurements of large wood will also contain, upon appropriate analysis, information about the spatial distribution of wood storage, and the covariation between wood storage and other important elements, such as alluvial sediment, topographic elevation (or height above river channel), channel and floodplain dimensions and morphological characteristics, or vegetation. At the location and scale of a single pixel, the occurrence and frequency of transitions between landcovers and landforms may yield information on specific processes such as recruitment and re-vegetation, and wood deposition and erosion. This approach will allow for the assessment of spatial distributions of wood deposition, such as concentrations (logjams) or dispersed pieces (i.e., individual logs) (e.g., Kraft et al. 2011), or the temporal aspects of large wood, such as persistence and analysis of transition. As such, the remote sensing approach will allow for assessments of spatial and temporal patterns of large wood and may be informative in studying flow divergence, bar sedimentation processes, and other geomorphic patterns and processes.

1.3. Objectives

We seek to develop a DL model to map large wood, alluvial sediment, water, and vegetation in an actively evolving river channel using a time series of high-resolution orthoimagery. With the resulting time-series data, we will quantify the magnitude and persistence (residence time) of the storage term of the time-varying wood and sediment budgets, as well as an analysis of transition among wood, sediment, water, and vegetation, which reveals the specific location of, or general likelihood of, temporal transitions that are the result of physical processes. We present both the novel methods

we have developed for generating maps of large wood, as well as a case study application of mapping large wood in a river undergoing significant and rapid changes because of an alteration of its wood and sediment regime by dam removal. This provides novel observations of the time-dependent effects of a large dam removal on the downstream fluvial geomorphology. It also serves as an example of how such data could in future be used to frame and test specific geomorphic hypotheses within the dataset's limitations, as well as an opportunity to discuss the limits of such applications. Finally, as will be demonstrated, our measurement target of total reach-wide large-wood area dictated an iterative, end-to-end approach to method development and applications.

We adopt a methodology similar to Sendrowski et al. (2023), who used a binary (wood / no wood) DL approach to pixelwise classification. However, we use different DL models, a different training strategy, on finer-resolution imagery and associated labeled datasets. Additionally, our models to detect and segment not just large wood, but also sediment, water, and vegetation. We compare and evaluate the use of four separate binary models for each class, as well as a single multiclass model that simultaneously predicts all four classes. Additionally, we have made our study reproducible by making our model training codes, trained models, training data, and codes used to generate and analyze the resulting maps, available in the hope that they may facilitate river-corridor mapping from high-resolution imagery acquired in other river systems. By our estimation, no prior large-wood study involving detection from imagery (Table 1) is computationally reproducible either because: (i) the wood was detected manually, and there is no present access to raw files, nor, in the majority of cases, a published schema that was employed to determine the presence/absence of large wood; (ii) the semi-automated processing scripts, if used, were not published and documented or are otherwise no longer available; or (iii) trained DL models and training data were not made publicly available.

We demonstrate that, as a monitoring tool applied to a time series of orthoimagery alone, and without the need for supporting datasets or in situ measurements, the DL method developed here allows for accurate measurements of wood-storage fluctuations and other spatial-temporal patterns resulting from dam removal. Further, high-

resolution photogrammetry of wood magnitude, persistence, and transport are combined with measurements of sediment to collectively reveal comprehensive observations of the coevolution of visible wood accumulations and sediment in the alluvial channel. Finally, we explore some of the implications of our observations from the Elwha River for understanding morphodynamic evolution of wood and sediment transport, a comparison of the responses of both reaches to their respective dam removal processes, and finally a discussion of the broader implications of our methods and findings for large-wood management and research. In this end-to-end study, we discuss what limitations our models have in these applications, imposed by our proposed methodology.

2. Study Site

We focus on two reaches of the lower Elwha River, which is situated on the Olympic Peninsula in western Washington, United States, and drains into the Strait of Juan de Fuca (Figure 1). Two large dams were built on the Elwha River during the early 20th century and removed nearly a century later as part of an ecosystem restoration project to reconnect anadromous fish with fluvial spawning habitats that were inaccessible because of the dams (McHenry et al., 1998; Pess et al., 2008; Duda et al., 2011). The forests that formerly occupied the site of the former Lake Mills and Lake Aldwell sites were logged prior to dam closure and reservoir filling, and the trees removed, but the root systems remained. The 32-m high Elwha Dam was constructed between 1911-1914 at ~7.4-rkm (river kilometers from the outlet) and resulted in the reservoir Lake Aldwell. Farther upstream, the 64-m high Glines Canyon Dam was constructed at ~21.6-rkm in 1927, impounding the Lake Mills reservoir. The lower Elwha Dam was fully removed between 2011 and 2012, and upper Glines Canyon Dam was removed incrementally between 2011 and 2014 (Ritchie et al., 2018a). The removal of these two dams resulted in the exposure of ~30-Mt of sediment deposited in the two reservoirs, two thirds of which (~20-Mt) subsequently eroded and was transported downstream by natural fluvial processes (Ritchie et al., 2018a). The restoration project reconnected the upper watershed, steep mountainous terrain of Olympic National Park, to the lower river and coastal sea, thereby allowing passage of sediment and wood from the upper

watershed to downstream reaches (Duda et al., 2008; Warrick et al., 2015; East et al., 2018; Ritchie et al., 2018a).

We use the river reach definitions of East et al. (2015, 2018), which define the 'middle reach' to be between the two dam sites, and the 'lower reach' to be downstream of the lower dam site (Figure 1). In our study, as described in Section 3, orthoimagery was publicly available for the two reaches downstream of former dams, but orthoimagery of the 9-km of former reservoir beds and deltas was not. The gravel-dominated (East et al., 2015, 2018) middle and lower reaches are ~8- and ~7-km in length, respectively, and the two reaches differ in terms of slope, elevation, sinuosity, and sediment conveyance (East et al., 2015, 2018). In the middle reach, the average gradient of the river channel varies between 0.007 and 0.009 at the sub-reach scale before entering the former Lake Aldwell delta and can be steeper in short canyon sections (East et al., 2018; Figure 1c). The lower reach, in contrast, is flatter with average gradients ranging between 0.004 to 0.007 with a wider active channel and a low-gradient river outlet region (~0.0013) that is just outside of our area of analysis (Figure 1c, d; Warrick et al., 2011; East et al., 2015). The geomorphology, sedimentology, and geological history of the Elwha River basin have been reviewed and described elsewhere (McHenry et al., 1998; Pohl, 2004; Duda et al. 2008; Pess et al., 2008; Latterell et al. 2008; Warrick et al., 2011, 2015; Draut et al., 2011; East et al., 2015, 2018; Ritchie et al., 2018a).

In addition to mobilizing ~20 Mt of sediment, an unquantified increase in wood was observed downstream and in the coastal zone following dam removal (Warrick et al., 2015, Ritchie et al., 2018a, East et al., 2018, and Bountry et al., 2018). Logjam area was suggested to increase, however, due to both the increase in large-wood flux from upstream observed at locations assumed to be representative, or from more comprehensive, but spatially limited, measurements (Warrick et al., 2015; DeMott, 2021). In addition, there is qualitative evidence that more local redistribution of wood (including some recruitment of floodplain trees) as the higher sediment load in the river led to increased lateral channel mobility and growth of sediment bars (East et al., 2015,

2018; Ritchie et al., 2018a). This increased influx and deposition of large wood followed an era of wood reduction in the Elwha River during the 20th century caused by wood sequestration in the two reservoirs and logjam removal, floodplain logging, and channelization of the river mainstem documented by McHenry et al. (1998), Duda et al. (2008), and Draut et al. (2011). In response to these historical reductions of large wood in the Elwha River, engineered logjams (ELJs) were built in the lower Elwha River by the Lower Elwha Klallam Tribe and partners between 1999 and 2010 to enhance floodplain connectivity, restore juvenile salmonid habitats, including scour pools that provide relatively cool water refugia, and mitigate bank erosion (McHenry et al., 2007; Pess et al., 2012). As shown below, we track the time-history of both non-ELJ and ELJ large wood in the Elwha River.

This history of large-wood abundance in the Elwha River catchment is similar to other steep, mountainous rivers of the Pacific Northwest region as documented by several studies (e.g., Abbe and Montgomery 1996, 2003; Montgomery et al., 1996; Haschenburger and Rice, 2004; Scott and Wohl, 2018). Historical reductions in wood abundance and distribution due to damming of lowland rivers, "…appear to have fundamentally changed the morphology, dynamics, and habitat abundance and characteristics of lowland rivers" (Collins et al., 2002) in the Pacific Northwest region. Additionally, wood currently entering Pacific Northwest rivers is generally smaller than historical log diameters and lengths, since most old growth forests have been logged in the region (Montgomery et al., 1996). The overall reduction in wood influx and size, coupled with wood harvesting from channels, has led to fewer, smaller logjams in most rivers in this region (McHenry et al., 1998). As a result, ELJs have been widely used in the Pacific Northwest in an attempt to decrease riverbank erosion and improve aquatic habitats (Abbe et al., 1997; Abbe and et al., 2003; Nagayama and Nakamura, 2010), ELJs may have had roles in the geomorphic evolution of channels through the recruitment of large wood into a mobile subpopulation or intermittently mobile subpopulation (Wohl et al., 2023). ELJs may also affect river-flow efficiency (McHenry et al., 2007) if they are large enough to create backwater effects. Thus, the Elwha River case study provides a unique opportunity to examine the supply, magnitude, timing, and persistence of wood under unusually high wood and sediment loading in a geographic

region where large wood plays a central role in the ecologic, hydrologic, and geomorphic setting.

Qualitative assessments of wood resulting from the dam removal project on the Elwha River suggested that wood distributions and abundances changed markedly along the downstream river channel, within the floodplain deposits, and along the shoreline near the river outlet following dam removal (Warrick et al., 2015; Draut and Ritchie, 2015; Shafroth et al., 2016; Ritchie et al., 2018a). An initial geospatial analysis indicated that the area of large-wood deposits had grown eight-fold between 2011 and 2016 in the Elwha River downstream of both dam sites (Bountry et al., 2018). Tracking of individually tagged pieces of large wood confirmed that wood traveled from both upstream reservoirs to the channel reach immediately downstream of both dams after their respective removals (Leung, 2019). While that the field component of that study focused on measuring sediment scour in the former reservoirs above the river reaches considered in this study, laboratory experiments were also conducted by Leung (2019) that shed light on the important role rapid wood deposition likely had in scouring pools in the gravel-dominated Elwha River system. These observations were corroborated by the hand-digitization of logs and log jams along the middle reach in a quasi-annual time series of orthoimagery, beginning August 2012 and ending February 2020 by DeMott (2021).

3. Data and Methods

Our methods include the development of a Deep Learning (DL) approach to detect not just large wood, but also sediment, water, and vegetation. We use a series of 14 published orthophotos from the middle and lower reaches of the Elwha River to detect large wood over a relatively large spatial extent (a total of 246-ha of active river channel, or 3444-ha over 14 surveys). This results in a greater temporal frequency (2.5 surveys per year) than most studies (Table 1). Automated methods for large-wood detection are necessary because, while conclusive, hand-based digitization of large wood in imagery is prohibitively time-consuming for quantifying total areal extents of the large wood from

a time series of imagery covering the entire active channel. Neither can these measurements provide information about the influences of large wood on channel morphodynamics, because the measurements result in information about large wood only, and not the evolving distributions of sediment, water, vegetation, and other landcovers and landforms. In addition, manual digitization of wood in imagery does not result in a computationally reproducible method, nor the development of an automated workflow that might be transferable to other contexts and studies. Finally, we note that careful manual digitization of wood is still prone to human error, but that error is difficult to quantify without comprehensive ground-based measurements of wood.

3.1. Orthoimagery

We relied on a series of aerial imagery collected as part of interdisciplinary before-after/control-impact studies of dam-removal response (Ritchie et al., 2018a, b). The orthoimagery data from Ritchie et al. (2018b) consist of 14 orthoimages of the middle and lower reaches collected between 2012-04-07 and 2017-09-22 (Figure 1). The published imagery represents a small subset of over 100 aerial surveys conducted between 2012-03-22 and present-day (the interested reader is referred to Supplemental Figure S1). A subset of our goals in this paper are to develop and present methods that result in a trained model that would be applicable to the entire 100+ survey record.

The orthoimagery was generated using SfM photogrammetry (Warrick et al., 2017; Spreitzer et al., 2019; Over et al., 2021) using a digital camera mounted in the wing of a small airplane. This time series of imagery from the two reaches downstream of the dam sites has previously been used by Ritchie et al. (2018a) and East et al. (2015, 2018) in geomorphic assessments of river-corridor changes. Example imagery from this time series for a small representative section of the middle reach is shown in Figure 2, revealing changes in the areal distributions of both large wood and sediment. A complete time series of this specific site in the Elwha River middle reach is provided in the Supplemental Information (Figure S2), which provides examples of the appearance of the channel under the varying light and weather conditions captured in the dataset.

Coincident and concurrent Digital Elevation Models (DEMs) of sufficient quality for fine-scale analysis are not available for this study, so our objective is to develop a technique for measuring the 2D accumulations of wood and sediment as apparent in high-resolution geospatial imagery alone, with no supporting elevation data or in situ measurements.

The 0.125 x 0.125-m pixel resolution imagery was reprojected in the NAD83(2011) / UTM zone 10N projection. We note that our orthoimagery are slightly larger than the 0.1-m pixel resolution threshold suggested by Ruiz-Villanueva et al. (2016) to accurately measure all large-wood pieces. While this threshold was determined by the defining diameter of 'large wood', most previous studies (Table 1) have used larger spatial resolutions to detect wood accumulations. Indeed, Taminga et al. (2015) tested their ability to manually identify wood by down-sampling their native 0.05-m pixel imagery, reporting that only beyond 0.8-m were pixels too large to accurately identify wood accumulations. Here, we find (and later report) that a great majority of accumulations of wood in the Elwha River consist of more than one piece and that we can detect many individual large-wood pieces. We also note that while the orthoimagery is of identical pixel size, it is of variable quality owing to improving cameras, camera mounts, and aerial survey methods in the first years of data collection (Ritchie et al., 2018).

3.2. Deep Learning label creation

The 28 orthoimages were split into 1024 x 1024 pixel tiles (each representing 128 x 128 m), with 50% overlap. This resulted in 45,878 image tiles for the middle reach, and 34,944 for the lower reach, or 80,822 image tiles in total. Labels were made using a Human-in-the-Loop image-labeling program, "Doodler" (Buscombe et al., 2021). Doodler facilitates relatively labor-free dense multiclass labeling of natural imagery, enabling relatively rapid training dataset creation for the four training classes (Figure 3 and Supplemental Figure S3). Each image can take between 5 and 15 minutes to label. Data labeling was iterative; several versions of the DL model were constructed over the course of two years, each time adding new labeled data and retraining/evaluating the

model output. This process only stopped when the model was deemed to be sufficiently accurate for the task. Ultimately, this decision was made using a comparative analysis of model-derived and ground-truth wood areas, outlined below in section 3.4. The final training dataset consisted of 4,382 image tiles and corresponding label tiles, each 1024 x 1024 pixels and representing just over 5% of the total dataset. The training data were sampled approximately equally in time and in space among both reaches. All training and validation samples purposefully included all four label classes (vegetation, water, sediment, and large wood), to avoid model training and evaluation problems associated with class imbalance (Buscombe and Goldstein, 2022). Class imbalance is the term given to a situation where the model sees many more examples from certain classes compared to others, which leads it to be over-confident about the majority class(es), and a problem that could have easily manifested in this study if image tiles were drawn at random. Instead, imagery was selected based on a two-stage process. The first stage ensured that candidate image tiles were drawn from a stratified random sample based on both equal sampling of time, and from all locations within the river corridor of both reaches. The second stage relied on the image annotator (primarily this manuscript's first author) to only label candidate imagery that upon brief visual inspection was determined to contain all four classes.

3.3. Deep Learning model training

We use the software package Segmentation Gym (Buscombe and Goldstein, 2022) to fine-tune a Segformer (Xie et al., 2021) DL model architecture for the task of semantic image segmentation. We take the instance (i.e., model architecture and trained weights) of the model of Xie et al. (2021), itself fine-tuned on the ADE20k dataset (Zhou et al., 2019) consisting of 512 x 512-pixel tiles and fine-tune it on our 1024 x 1024-pixel training data. This is an example of the benefits of so-called transfer learning (Zhang et al., 2022), where one model instance trained for a specific task (i.e., to recognize classes in the ADE20k dataset) is fine-tuned to meet the needs of a similar task (i.e., trained under supervision to recognize the classes of a different labeled image dataset). This is achieved by initializing the model with the weights of the old dataset, modifying the last

layer of the model to specify the new target classes and then iteratively adjusting the weights of the model during training using the new dataset.

Segmentation Gym allows for full reproducibility in the process of training or fine-tuning and evaluating image segmentation models, as well as hyperparameter experimentation for the purposes of optimizing trained models, as described by Buscombe and Goldstein (2022). The SegFormer model architecture was used, which includes a hierarchical Transformer architecture, called "Mix Transformer," as an encoder that extracts features from imagery, and a decoder for segmentation that uses those features for class probability estimation. The Mix Transformer is built around the concept of self-attention (Vaswani et al., 2017), specifically, a spatial self-attention layer. At a high level, a self-attention layer works in a similar way to convolution layers, highlights the salient spatial areas of the imagery important for feature extraction and prediction, while suppressing the irrelevant image portions for more contextualized predictions. It yields state-of-the-art performance while being more efficient to train than existing models (Rußwurm and Körner, 2020; Khan et al., 2022).

The segmentation example provided in Buscombe and Goldstein (2022) was an example of a model designed to generalize well to locations outside of the training dataset; it, therefore, had relatively large numbers of samples for validation and relatively few for training. The reasoning for the abundance of validation data was to simulate a test set with a wider range of environmental conditions. In contrast, the concern with the present application is to segment imagery within a relatively small range of locations and times. While there is still considerable variability among sites and times owing to changing light, river color due to suspended sediment, river stage, and vegetation leaf conditions, we reasoned that model building would be improved with more emphasis on training samples than validation samples. In this manner, the model saw more of the data it will later, in effect, extrapolate over; thus, a smaller validation set was dictated. Therefore, the labeled images were further split into 3068 training and 1314 validation images. Unlike Buscombe and Goldstein (2022), who used augmented sets of training and validation imagery, here we used augmentation only on the training imagery to give the model more training data to generalize to, and to avoid the

possibility of mis-representing validation statistics by using transformed validation imagery. Augmentation consisted of random horizontal and vertical flips of imagery, as well as shifts in horizontal pixels of up to 10% of the image width, and rotations up to five degrees. The final training dataset consisted of 18,408 training and 1314 validation samples.

We did not know in advance if wood detection would be better by a model trained only for that task, i.e., trained using binary labels of wood/other, or alternatively by a model trained to estimate all four classes (water, sediment, wood, vegetation) simultaneously. We therefore trained a multiclass and a set of binary models to compare approaches, evaluated in terms of the ability to detect wood. One consideration is to what extent the model needs a given class in the greater context of the adjacent classes; if this need is greater, we expected the multiclass model to perform better. Several model instances were trained for each case by varying the learning rate (Figure 4 and Supplemental Figure S4). All models converged well. In general, we found that a low learning rate ($1e^{-8}$) was optimal. The only hyperparameter we varied was the learning rate. Models were trained using a minibatch size of 12, the maximum size we could distribute across two RTX 3090 Graphics Processing Units, and model training typically converged within 10-20 epochs (Figure 4; one training epoch typically completed within 30 minutes).

We used multiple standard metrics to evaluate segmentation model outputs, namely overall accuracy, frequency weighted Intersection over Union (fwIOU; Long et al., 2015), mean Intersection over Union (mIOU; Buscombe and Goldstein, 2022), Matthew's Correlation Coefficient (MCC; Matthews, 1975), Precision, Recall, and F1 score, which are all standard evaluation metrics in applications of Machine Learning models (Maxwell et al., 2021). These quantify different aspects of the correspondence between observed and estimated wood pixels, leading Buscombe and Goldstein (2022) to conclude that keeping track of multiple metrics is optimal for final accuracy assessment as well as operational concerns such as monitoring model performance upon successive retraining with new data.

For comparisons among several models able to predict the same class, we found MCC better reflected the error rate visible to the eye than either mIOU and fwIOU, possibly because, to yield a high MCC, relatively high scores are required for true negatives and positives, potentially ameliorating the problem of high recall (note that a model producing no false negatives has a recall of 1.0, which masks the low precision, anda model producing no false positives has a precision of 1.0), and vice-versa, in F1 scores, which are the harmonic means of recall and precision scores (Maxwell et al., 2021). We also noted qualitative improvements in the visual assessment of outputs of the four-class model, which tended to suffer from less egregious errors than the binary models (whose model-training curves are shown in Supplemental Figure S4). We therefore chose to use the four-class model (Figure 4), which has a high MCC (Table 2), and is also more practical to apply than three separate models. From there, we evaluated Recall, Precision, and F1 score to compare the per-class error rate for the four-class model (Table 3). However, we observe that these scores are heavily class-imbalanced (i.e., biased low for relatively rare wood and sediment, and high for relatively common water and vegetation classes). Ultimately, because this model is constructed primarily as a measurement tool for quantifying wood, and the major focus of this contribution is to use the model outputs to better understand the dynamics of wood in the system, the accuracy of the model must also be understood principally in terms of the ability to estimate wood load over every spatial scale, and for the entire time period captured by the data. Therefore, the comparison of model-derived and ground-truth wood areas, outlined below in section 3.4, is the most important model evaluation metric.

For each orthoimage, we used the digitized channel margins and river thalweg locations previously developed by East et al. (2018) to define the study area. The maximum extent of these combined channel margins was used to clip the extent of all model outputs. For ground-truth purposes, we hand-digitized all wood visible at 1:300 scale in four out of the 28 orthoimages: the first and last surveys in the record for both the middle reach and the lower reach. The digitizing scale was chosen to mimic the scaling of the orthoimage tiles used to train the model. These wood polygons were rasterized at the orthophoto resolution to be consistent with our gridded DL products. There is some unquantifiable bias associated with this tedious digitization process, but

we estimate that is well within 10% of the true areal extent of wood accumulations visible at the surface. To demonstrate change in model performance as a function of number of label images, separate four-class models were trained on datasets based on 999, 1999, 2999, and 4382 images, all with the same hyperparameters. Minimum validation loss, which is the final validation loss of the trained model on completion of training, decreased with the number of images (Figure 4), and all validation metrics increased (Figure 4). The MCC is, overall, the most sensitive metric for measuring model improvement with more available training data. Validation scores increased linearly with number of images (dashed lines in Figure 4c), whereas training scores plateaued after 1999 labeled images. Training scores remained higher than validation scores, a reflection of our decision to provide the model with relatively more training data than validation data. Given much more model training experiments involving different proportional splits between training and validation subsets, the optimal split between training and validation would be equal numbers of training and validation scores (MCC or other metrics). It is difficult to develop an intuition for importance of these metrics because they vary from task to tasks and do not scale with convenient variables such as dataset size, or number of classes. In practice, the metrics track relative progress of the model undergoing training under different scenarios (for example, different/more data, or different hyperparameter choices) and are useful for determining when to stop labeling data, which is of enormous practical importance because labeling is time-consuming. However, ultimately, as we note above, in this study we conducted an independent assessment of absolute model skill with respect to large-wood detection.

3.4. Image segmentation: Model implementation

The four-class segmentation model was applied to each image tile and results in the overlapping regions were averaged with Lanczos resampling (e.g., Duchon, 1979) to enhance local contrast of classes at their mutual boundaries. Overlapping tiles were then recombined into a full-size orthoimage (i.e., the same extent and size as the original imagery) mosaicked into four raster bands, one per class. These per-pixel, spatially

averaged class probability maps were written to GeoTIFF format files, and the files representing per-class probabilities. The argmax (argument maximum) operator was used to determine the class for each pixel in overlapping sections (Supplemental Figure S5). We used the four-class predictions for data visualization and transition analyses (section 3.7.), and the wood and sediment predictions for further analysis of the evolving spatio-temporal distributions of wood and sediment.

3.5. Model wood detection evaluation

All visible large wood in the active channel was manually digitized in four orthoimages of the study area, as noted in Section 3.1, consisting of accumulations of wood (wood pile/jam), and including larger visible individual pieces, which we note were mostly trunks of former trees. These image features were digitized at 1:200 scale in a GIS as polygons capturing the area of each wood accumulation, then rasterized at 0.125m pixel size, the same as the orthoimagery. These spatially comprehensive data were used as ground truth to evaluate the ability of the DL models to detect large wood. Observed and estimated reach-scale wood abundances were within 15% (Figure 5a), with differences of 14.09 and 14.32% for the middle and lower reaches, respectively, in 2012-04-07, and 13.28 and 14.6% in 2017-09-22. Similarly, the observed and estimated size-distributions of wood areas compare closely (Figure 5b and c), which suggests that the model is good at detecting both smaller and larger wood pieces and piles without any systematic bias. Cumulative abundances as a function of distance downstream in both reaches also track well, showing that error is accumulated throughout both reaches at a quasi-constant rate of about 15% (Figure 5d and e). We therefore use this nominal, slightly conservative, error rate of 15% for the entire spatio-temporal extent of the data, which reflects a zero bias in both space and time. We argue that this is a significant achievement considering the large variability caused by changing light, vegetation state, water color, amount of whitewater, and other factors that varied through the imagery time series (see Supplemental Figure S2).

3.6. Metrics describing the magnitude, covariance, persistence of large wood

Large-wood magnitude is commonly reported as volume of wood per unit area and referred to as wood load (Van der Nat et al. 2003). However, measuring the thickness and porosity of wood accumulations still represents a major challenge (Campbell et al., 2019; Spreitzer et al., 2019; Livers et al., 2020). These quantities likely vary considerably in space and time due to natural variations resulting from transport and deposition processes, wood attrition and recruitment, and the diversity of the assemblage tree species and sizes (Campbell et al., 2019). Prior field-based and on-screen measurements of wood in the Elwha River system (Leung, 2019; DeMott, 2021) strongly suggest a significant variation in wood thickness. Leung (2019) estimated a 15% error rate in the specification of any dimensions of a large-wood deposit, and such an error would quickly accumulate over an entire reach, especially when combined with an accumulation of a 15% error rate for wood detection. Neither the Leung (2019) nor the DeMott (2021) studies examined porosity of large-wood deposits. The thickness and porosity of a given wood accumulation cannot be derived with confidence from imagery alone, even though previous remote sensing studies have made these estimates using sphere approximations (e.g., Ulloa et al. 2015; Sanhueza et al., 2019) or using estimates of wood height (or thickness) and porosity (e.g., Livers et al., 2020; Livers and Wohl, 2021; Boivin et al., 2015). Finally, we note that DeMott (2021), who reported their Elwha River wood measurements as areas for possibly the same reasons as listed above and were nonetheless able to draw convincing conclusions from their data regarding wood distributions in the middle reach. Ours is an evolution of the workflow demonstrated by DeMott (2021).

Our measurements of wood area were derived exclusively from enumerating wood pixels in the segmented imagery. Because we lack reliable information on the height and porosity of wood accumulations in the study area, we chose not to adopt the common approach of converting area to volume. Additionally, we have no basis to assume that average wood thickness or porosity values from other studies would apply to our study area, especially owing to the strong – and potentially unique – time-dependent patterns in large wood caused by the Elwha River dam removals, and a lack of applicable

knowledge of typical porosity and height values for wood accumulations of specific tree species (cf. Campbell et al., 2019). For some of our analyses, areas have been normalized by subregion of the active channel areas to provide the proportion of the active channel covered by large wood or sediment (m^2/m^2, or %). This normalization was done within subregions by subdividing the active channel into 52 units in the longer middle reach and 44 units in the shorter lower reach that averaged 200 m in the along-channel direction. These regions were delineated in a GIS using the digitized channel margins (polygons) previously developed by East et al. (2018). These measurements of large-wood areas were obtained during low flow in the river (Figure S6, Figure S7a,b,c), and there was no significant correlation between estimated wood areas and flow (r^2 = 0.11 and 0.23 for lower reach and middle reaches, respectively; Figure S7d), indicating that fluctuations in river stage did not significantly influence our results and interpretations. The discharge at time of the orthophoto surveys was always below the 25th percentile of the 5-year daily record for the study period (Figure S7c). While we chose low discharge imagery, discharge was nonetheless variable. Additionally, bars were growing, and a stage-discharge relationship is not available owing to the dramatic and rapid changes to channel morphology, as documented by East et al. (2015, 2018). Therefore, we do not know the change in exposed area as a function of variable discharge for each individual orthoimage, but we can estimate it to be small. As East et al. (2018) and Ritchie et al (2018) report, bars grew significantly in place because of the 20Mt sediment pulse due to dam removal, and this is very evident in the imagery. Bar exposure and channelization in the imagery is decoupled from fluctuations in stage, making time-series measurements meaningful. Because we measured both the increase in planform areal accumulations of subaerial wood and sediment, as they occurred together, from the same imagery, the relative abundance of the two quantities are directly comparable. That said, it should be acknowledge that there is potentially a submerged/buried component of total wood storage that is missed by our measurements, as well as a small potential low-elevation wood component due to fluctuations in stage.

The geospatial data generated from the DL analyses were also combined into a 3D timestack of maps to assess multiple factors of the data at a specific spatial scale and over a specific time period. Our analyses include large-wood distributions, magnitudes,

and persistence, but they also include relationships between the deposition of large wood and sediment and the mode of wood storage. Wood persistence was quantified at a pixel level as the cumulative sum of wood for a given pixel. Maps of these cumulative sums provide an easily interpretable visual assessment. Wood-sediment relationships were assessed with the covariance between the respective time series of wood and sediment magnitudes. Covariance was quantified using both wood-to-sediment and normalized wood-to-sediment ratios, as well as correlation analyses. Normalization involved dividing the wood and sediment areas by their respective sums, then computing the ratio of the two normalized quantities.

Notably, controlling for river stage fluctuations in areal estimates would be possible if a stage-discharge relation could be obtained for this time-period. In practice, this would be very difficult to achieve owing to the rapid channel change observed by East et al. (2015, 2018). That said, because we used relatively low-stage imagery only, and the very wide range of heights above river thalweg elevation where wood is deposited, we estimate the variance in wood area estimates due to stage fluctuations to be a few percent at most. In addition, while it is acknowledged above (and in Ritchie et al., 2018) that image quality was variable, in the end that variability in image quality was shown not to have a significant impact on wood detection accuracy, because the relatively low quality early 2012 imagery and the relatively high quality 2017 imagery both yield similar accuracies (Figure 5a).

3.7. *Transition analysis and Markov chain model*

The 14-point time series representing the time-history of 13 discrete state-transitions at every location in the river corridor is amenable to transition analyses. Transition probability matrices are a common tool used to describe the likelihood of discrete state changes in environmental systems (e.g., Davis and Sampson, 1986; Fieberg and Ellner, 2001; Takada et al., 2010). Here a state change from one class to another, e.g., water to sediment or vice-versa would imply a reversible state change, i.e., sediment deposition/erosion. A self-transition, such as wood to wood, is a direct measure of persistence. The frequencies are compiled for each transition from each class to every other class. Because there are four classes, a 4 x 4 transition probability matrix was

made to represent the empirical likelihoods of 16 possible processes encoded at every pixel location and every timestep. Here they are used to examine the likelihood of individually relevant changes in state, for example, from sediment to wood which indicates wood deposition, or from sediment to vegetation which indicates vegetation growth and sediment stabilization. Additionally, they are used to show downstream trends in transitions, and reach-wide differences in average behavior (a 'fingerprint' of the system).

The timing of the present study is such that it covers the tail-end of the period of dam removal, which began in 2011, and the subsequent rapid evolution of the system toward a new state (DeMott, 2021). Transitions in the Elwha River system are amenable to stochastic analyses of our dataset, such as Markov chain analyses, that may capture this transition to a new equilibrium state for each class and across each reach and sub-reach. The steady state probability distribution, computed using a Markov chain model constructed from a transition probability matrix, describes the system which converged to a point where the transition probability distributions will no longer change. In other words, the time-invariant probabilities of a change to or from vegetation, water, sediment, and wood. This distribution does not depend on the absolute amount of any class.

A time-homogenous Markov chain is defined in terms of the probability distribution of state transitions. Specifically, the probability distribution of states at time step $t+k$ is given in terms of its distribution at time t by (Davis and Sampson, 1986),

$$\pi(t+k) = \pi(t)P^k, \qquad (1)$$

where all information about the evolution of the probability distribution of m states is contained in the $m \times m$ transition probability matrix, P, a row-stochastic matrix where all rows sum to 1. The probability distribution π is the steady-state distribution. If Markov Chain theory holds, the k-step transition matrix should be approximately P^k. This presents an opportunity to use the Markov chain to test for the hypothesis of equilibrium, by comparing individual $P(t+k)$ compiled from the data, with P^k determined from (1). The steady-state distribution satisfies

$$\pi = \pi P, \quad (2)$$

where π is computed as the left eigenvector of P (the eigenvector associated with an eigenvalue of 1).

We compile P for each sub-reach of the middle and lower river reaches, using the same sub-reach system as used for computed normalized wood and sediment area measurements. To compare the average tendencies of class transitions in both reaches, we computed the mean probability transition matrix by aggregating transition frequency matrices per sub-reach, before normalizing by reach-wide frequencies of each class to estimate the average P per reach. Transition data per sub-reach are also visualized as a function of downstream distance. Finally, we compute and compare π for each reach to examine and discuss any reach-wide differences in the steady-state probability distribution. Similar analyses were employed by Senter and Pasternack (2011) to examine the role of large wood in salmonid spawning habitat.

3.8. Supporting data

The Lower Elwha Klallam Tribe has overseen the construction of engineered log jams (ELJs) in the lower reach and have collected data on several channel attributes in and around the ELJs. The Lower Elwha Klallam Tribe data used here includes construction date and location of ELJs, and maximum pool depths and bar grain size distributions in the vicinity of ELJs, which were obtained at various times between 2001 and 2021. Grain-size distributions were determined using a standard Wolman count based on randomly selected surface particles (n=100). Lastly, river discharge and sediment load measurements during the period come from Ritchie et al. (2018b). These data quantify fluxes of water, suspended sediment, and bedload sediment at U.S. Geological Survey gaging station 12046260 (U.S. Geological Survey, 2023), which is downstream of the two former dams (~1.5-km downstream of Elwha Dam site, Figure 1).

4. Results

4.1. Large wood and sediment abundance

The labeled imagery provides detailed time histories of the evolution of the Elwha River channel margin during and after dam removal, and example DL results from several channel reaches are provided in Figure 6 highlighting only the net change over the 5.5-year study period. In general, the imagery and its DL segmentation show that all channel sediment bars expanded in size and position over the orthoimagery record, and that the amount and distribution of large wood also changed markedly on every bar, often several times during the 5.5-year time series (Figure 6). Common patterns of changes to the fluvial landscape include: (i) wood deposition concentrated at the upstream apex of bars constraining flow, (ii) river channel position changes associated with appearance of new wood deposition, and (iii) a decrease in the areal extent of vegetation and water, which are consistent with the observations of Ritchie et al. (2018a) and East et al. (2018). There was no evidence of any channel-spanning log jams, nor observable hydraulic backwater effects (cf. Livers and Wohl, 2021) associated with wood accumulations and no evidence of wood rafts that completely blocked the active channel (Boivin et al., 2015). Only a negligible (estimated <1%) amount of wood was detected in the channel, presumably undergoing active transport at the time of survey (and could possibly be further isolated and studied by finding wood pixels surrounded by water pixels).

The average spatial patterns of large wood and sediment provide an overview of where accumulations were found, and how this spatial distribution changed in time (Figure 7). In the middle reach, large wood was concentrated near the center of the reach, where it reached total areal maxima at about 16-rkm (Figure 7a). In the lower reach, total large-wood abundance tended to increase in the downstream direction resulting in areal maxima in the wider, lower-gradient distal end near the river outlet (0- to 5-rkm; Figure 7a). The total area of both large wood and sediment as a function of distance along the river were highly correlated (Table 4) because almost all large wood was deposited on bars (Figure 7b), rather than in the relatively short canyon sections where wood is occasionally found in riffles. The linear correlation (r) of these time-

averaged wood and sediment areal values across the 96 subregions presented in Figure 7 was 0.88 and 0.92 in the middle and lower reaches, respectively (Table 4). Correlations between the time series of reach-wide wood and sediment areas are also high (r=0.86 and 0.77, for middle and lower reaches, respectively; Table 4), but slightly lower than correlations over downstream distance. Finally, time series of wood in the two reaches also display a high correlation (r=0.78), as do time series of sediment (r=0.89), suggesting that both reaches responded similarly to the same upstream sediment and flow boundary condition without significant time lags. These results suggest strong colocation relations between the sediment bars and deposits of large wood, which we will explore more fully below.

Reach-wide totals of areal values of large wood and sediment changed significantly over time (Figure 8). Whereas wood magnitudes plateaued in both reaches in 2014 or 2015, the sediment areas in these reaches continued to increase through at least the winter of 2016/17 (Figure 8a, b). Large-wood areas increased from around 15,000 m^2 in the middle reach and 20,000 m^2 in the lower reach to approximately 35,000 m^2 in both reaches, most of which occurred between April 2012 and the winter of 2014 (Figure 8b). In contrast, areas of deposited sediment increased from 100,000 m^2 in the middle reach and nearly 200,000 m^2 in the lower reach, to ~250,000 m^2 in both reaches by 2014 and to more than 300,000 m^2 in both reaches by 2017 (Figure 8b). These up to four-fold increases in the areal extents of both large wood and sediment greatly exceed measurement uncertainties of ~15%. Over the study period, the middle reach saw largest net proportional increases in wood and sediment, with 2.3-times more wood, and 3.5-times more sediment at the end of the study period than at the start. The equivalent net increases for the lower reach were a 1.75-fold increase in wood and 1.5-fold increase in sediment. Although the time series of both quantities in both reaches are similar in magnitude, the lower reach saw greater net increases in wood, whereas the middle reach saw greater net increases in sediment.

Further examination of the correlation between the areal extents of large wood and sediment suggests that the ratio of large wood to sediment declined over time (Figure 8c, d). For example, the ratio of wood to sediment peaked at 0.175 in the middle reach in

July 2012 and declined to less than 0.1 by September 2017 (Figure 8c, d). In the lower reach, the wood-to-sediment ratios declined from 0.16 to 0.10 in the same interval of time. Normalized wood-to-sediment ratios show a very similar pattern, although these data show that the overall normalized ratio of wood-to-sediment in the middle reach was about 50% greater than the values measured in the lower reach (Figure 8b, d). Overall, this suggests that total areal extent of the exposed sediment on the channel bars continued to increase after the area of wood deposition had plateaued.

A more detailed examination of the spatial and temporal context of large wood and sediment abundance is provided in the matrices shown in Figure 9, where the data are presented as raw areal values (upper figures) and normalized areas by including the local channel corridor areas of East et al. (2018) (lower figures). Normalizing these areal measurements reveals that sediment commonly dominated the channel area following the influx of 2012-2013, when it regularly exceeded 50% of this area (Figure 9d). Large wood typically covered ~5% of the channel area, although the largest wood accumulations could cover up to 25% of the channel area in some sub-reaches (Figure 9c). The temporal fluctuations in large wood and sediment reveal several localized deposition events in both the middle and lower reaches, where wood areas increased 2 to 10-fold during the events (Figure 9; events highlighted with arrows). For example, several localized increases in wood abundance were observed in the middle reach during 2013 and 2014, and another large-wood-deposition event occurred at 17- and 18.5-rkm in 2016 (Figure 9a,c). The event-based deposition in sediment is similar in timing and location to the event-based deposition of large wood, suggesting that these two phenomena are coincident (Figure 9).

4.2. Persistence and size distributions of large wood

We visualized spatial persistence by enumerating each grid cell with the proportion of time that location was occupied by wood. In this analysis, the ever-persistent wood piles will have a value of 1 and may be long-standing natural logjams or ELJs, whereas values of 0.5 indicate that wood had been present half of the time. Examination of the

temporal patterns of wood within the Elwha River channel margins revealed several patterns of persistence, exemplified qualitatively in Figure 10 (and Supplemental Figure S8). Some channel reaches exhibited more spatially dispersed accumulations of wood, for which wood pieces were observed to be individual pieces of accumulations of only several logs (Figure 10 and Figure S8).

Naturally, such analyses applied to a higher-frequency time series would result in more specific pinpointing of change, as well as capturing high-frequency changes. Therefore, we focus on the reach-wide trends of wood size distributions to examine the general tendencies in each reach for comparative purposes. The time series of reach-averaged wood-accumulation size distributions show similar trends, with the coarse tail of the wood-accumulation size distributions relatively depleted in 2012, then enriched by 2014, then relatively depleted again thereafter (Figure 11a, b). Wood-accumulation size distributions are exponentially distributed in both reaches with an exponential fit explaining all but the smallest wood pieces and piles (Figure 11c). This observation may be useful for developing models for large-wood size distributions in similar rivers. Mean wood accumulation area varied between 7- and 24-m^2 over the study period (Figure 11d), increasing rapidly until its peak in summer 2013 and decreasing slowly thereafter. This general pattern was stronger in the middle reach and weaker in the lower reach.

4.3. Engineered Log Jams

The dynamics of wood in the vicinity of known ELJs in the lower reach was investigated to determine whether the DL techniques could adequately map and characterize these features and to assess the time history of the 55 structures during channel adjustments such as avulsions and bar building that resulted from dam removal. Active ELJs are defined as those with wood accumulations within a 5-m radius at time of aerial survey. Several ELJs constructed prior to dam removal were already gone (or not detectable because of obscuration by vegetation) by the start of the present study in April 2012 (Figure 12a, c). The amount of large wood in the reach that was deposited outside of the ELJs was far greater than the wood deposited in the vicinity of

ELJs (Figure 12b), especially in the Hunt Road channel or western anabranch (a major anabranch ~1-km long in the lower reach that became the mainstem channel after a 2007 flood; Draut et al., 2011). However, extra-large-wood deposition did occur at the three ELJs from the pre-dam era that persisted until September 2017 (Figure 12c). The number of detectable ELJs within the river channel margins declined over time from nine in 2012 to three in 2018 (Figure 12d). We note that several of the ELJs may have been obscured under canopy, and their persistence or disaggregation was not captured so their fate is uncertain. However, they likely are playing a less important role in river morphodynamics because many are demonstrably gone, and those remaining but obscured by canopy may now be disconnected from the river under most flows.

4.4. Channel characteristics in the vicinity of wood accumulations

Time-series measurements of numerous alluvial bars in the lower reach made by the Lower Elwha Klallam Tribe reveal a dramatic overall fining of alluvial bars until 2014, then a subsequent coarsening of those bars until 2021 (Figure 13b). This is consistent with hundreds of field measurements of surface grain size made in three sub-reaches of the lower reach by East et al. (2018; their Figure 4), where sediment fined greatly in 2011–2014 compared to the dammed condition (measurements from 2006 to 2011). Grain size coarsened gradually after 2015 but remained finer than in its dammed state by 2017 (East et al., 2018). This indicated that the peak of the sediment pulse from upstream reservoirs has passed through this location, and that the river had returned to a supply-limited state after having been transport-limited during the peak of the sediment pulse (East et al., 2015, 2018). However, mean wood rack volume increased steadily until 2018 (Figure 13c), as did pool depth until 2021 (Figure 13c). We also observed a decline in mean pool depth in 2014/2015 coincident with peak sediment transport, and then a deepening trend to 2021 (Figure 13d).

4.5. Transition analysis

The full- and sub-reach scale transition probability matrices and steady state probability vectors were computed for both reaches following the methods outlined in section 3.7. A comparative analysis of reach-wide transitions is presented in Figure 14. Each matrix can be viewed as encapsulating the likelihoods of 16 unique processes associated with channel change (Figure 14c). In addition, the differential between the respective probabilities in middle- and lower-reach matrices (Figure 14d) provides a ready means with which to contrast the two reaches in terms of the relative importance of each process in each reach. The reach-averaged transition matrix, *P*, for the middle reach (Figure 14a) and lower reach (Figure 14b) display significant differences in the probabilities of transition between several classes. Middle reach wood is globally more persistent, with a self-transition probability of 0.24 compared to 0.18 in the lower reach. Lower reach sediment is less persistent, with a value of 0.43 compared to 0.51 in the middle reach. Among other noteworthy differences are those for vegetation to wood transitions, many of which are due to vegetation removal and subsequent wood deposition in that location, processes which are twice as likely in the middle reach (0.24) compared to the lower reach (0.12).

Transition probabilities for each of the 16 processes at sub-reach scale are summarized in Supplemental Figure S9, providing a comprehensive picture of the occurrences and rates of individual processes as a function of downstream distance. Persistence in wood can be highly localized in both reaches (Figure S9a). Wood persistence is generally associated with high persistence of sediment at sub-reach scales, especially in the middle reach. Persistent wood in the lower reach is more spatially variable (spatial variability value of 1.0) than in the middle reach (0.86; Figure 14e, f).

The prevalence of processes that add or remove wood also vary considerably with distance downstream (Figure S9c, d). However, it is apparent that wood deposition rates in locations previously occupied by water are substantially higher in the lower reach (Figure S9c), as are wood removal rates. In short, there is a greater rate of transition from water to wood and vice-versa in the lower reach compared to the middle reach. Conversely, the rate of transition from vegetation to wood, and vice-versa, are significantly more common in sub-reaches of the middle reach, compared the lower

reach. These data suggest that the coincident enlargement of bars and wood deposition in the middle reach occurred predominantly in portions of the floodplain that were previously vegetated, whereas wood/sediment deposition in the lower reach predominantly occurred in areas previously occupied by river channel. These are the reasons why the inter-reach probability divergence values for vegetation to wood, and vegetation to water, are large (Figure 14d).

The steady-state vectors for both reaches were computed following section 3.7. These vectors represent the time-invariant probabilities of states in a system assumed to be in steady state (equilibrium), or the long-term likelihood of transitioning to/from a class. In the middle reach, π = 0.57, 0.048, 0.22, 0.17 for vegetation, water, sediment, and wood, respectively. The same vector for the lower reach is π = 0.65, 0.07, 0.07, 0.21. The values indicate a degree of similarity in tendencies for transitions to vegetation, water, and wood. The most significant finding is that 17 and 21% of transitions in the middle and lower reaches, respectively, involve large wood, underlining its abundance and dynamism, and therefore potential importance in the morphodynamics of this river. The most notable difference is the comparatively low value for lower reach sediment (0.07) compared to that in the middle reach (0.22). These steady state probability vectors may be viewed as a fingerprint of the system at hypothetical equilibrium. Neither reach is a closed system with respect to large wood and sediment due to transport into and out of either reach, e.g., wood can be recruited from floodplain areas during channel migration and high flows, and wood in transport could also be deposited on the floodplain. With no indication that the lower reach was more out of equilibrium than the middle reach, the relatively low value for steady state sediment probability may reflect the fact that the lower reach saw greater net increases in wood compared to sediment (Figure 8) and that sediment in the lower reach is less persistent than in the middle reach (Figure 14). Like many of the complementary comparative analyses presented here between the two reaches, the respective reach-wide steady state probability vectors encapsulate both the similarities and differences of landcover distribution dynamics, which are summarized using all lines of evidence in section 5.2.

5. Discussion

The new deep-learning methods utilized in this study provide for an unprecedented level of detail in the evolution of large wood in the Elwha River corridor over multiple years and tens of kilometers. These methods were more effective when developed with spatially integrated metrics of large-wood abundance gleaned from careful manual digitization of wood in imagery that bracket the entire study period. Segmentation of large wood in imagery was also more successful when considered one class in a 4-part segmentation schema. Moreover, the unique opportunity to study a river undergoing a planned major pulse of sediment and wood during the world's largest dam removal to date provides a unique before-after investigation of large-wood movement. Below, we explore some of the implications of our observations from the Elwha River for understanding morphodynamic evolution of wood and sediment transport, a comparison of the responses of both reaches to their respective dam removal processes, and finally a discussion of the broader implications of our methods and findings for large-wood management and research.

5.1. Suitability and expansion of the deep learning approach

The results presented here were not our first attempt at successfully training a DL-based image segmentation model for Elwha River imagery. In fact, the process took over 2 years, with several iterations of labeling data creation and model training and testing. While DL-based image segmentation is more accessible than ever, there is still a significant amount of work involved in data labeling, model selection, hyperparameter selection, multi-metric model evaluation, and application to large spatial scale imagery, as documented in the present study. These details are the difference between success and failure, and ours may serve as a generally useful case study for image segmentation at high resolution and large spatial scales. Previous attempts to train a Residual UNet architecture used by Buscombe and Goldstein (2022) from scratch on this training dataset resulted in a significantly worse performance and model convergence times, which is why the SegFormer model was ultimately used. The two model architectures

crucially differ in terms of number of parameters, with the Residual UNet model having far fewer parameters because it consists only of convolutional layers, rather than fully connected layers (otherwise known as a perceptron in the parlance of traditional artificial neural networks), which have more parameters (Buscombe and Goldstein, 2022). The SegFormer model uses a fully connected decoder layer for classification, which we partially attribute to its success; it has far more parameters with which to make predictions, and the fully connected nature of the classifying layer means it can resolve classes at finer resolution. It is also possible that the basic image feature extraction process that the SegFormer uses to make predictions, the so-called self-attention layer (e.g., Aleissaee et al., 2023), is more effective than the convolution layers used by the Residual UNet for the same task, which is consistent with earlier model comparison work using remotely sensed data such as Rußwurm and Körner (2020) but would require further investigation to verify. So-called DL 'model explainability' and model-calibration methods for image segmentation are still in their infancy (e.g., Linardatos et al., 2020), which makes it difficult to assess factors such as what image regions are important, and how under- or over-confident a model prediction may be for each class.

Deep learning models typically require large volumes of labeled training data; the only other known example of large-wood detection using automated supervised deep learning methods, namely that of Sendrowski et al. (2023), used 10,053 hand-labeled image tiles. However, once the model is trained on a larger number of examples, it is much more robust to noise than other available methods. Given the relative differences in study area (Table 1), our training data consist of between 5 and 25 labeled images per hectare depending on the amount of labeled imagery used for the model (Figure 5f), and that of Sendrowski et al. (2023) consists of an estimated 0.28 labeled images per hectare. It would be beneficial to combine labeled datasets and train new wood-detection models under Transfer Learning scenarios where multiple sources of imagery are available, such as to construct time series from disparate image sources and times.

In this study, our use of the argmax operator to determine most probable per-pixel class as the one with the largest probability was a standard approach in image

segmentation (Buscombe and Goldstein, 2022). However, this approach does not provide an associated measure of relative uncertainty of each estimate, such as the post-hoc classification of an 'uncertain' or 'unknown' class where probabilities do not hit a threshold, which could be addressed in future work. Additionally, the use of coincident elevation data in future work would lead to a greater understanding of wood deposits in relation to the elevation of river level. Digital surface models (DSMs) from LiDAR or SfM photogrammetry would be a valuable additional data source (e.g., Kasprak et al., 2012; Spreitzer et al., 2019; Sanhueza et al., 2022).

5.2. Morphodynamics of Elwha River wood and sediment

Large-wood deposition in the Elwha River floodplain increased significantly between the start of dam removal (2011) and winter 2013, then plateaued (Figure 8b). This is broadly consistent with the less spatially extensive analysis of DeMott (2021) that revealed that the total number of individual logs initially increased by approximately four-fold during the first year after dam removal (i.e., 2012 - 2016) before returning to background levels, while the total log-jam area along the middle reach increased between 2012 and 2020. This pulse in wood occurred simultaneously in the lower reach and middle reach during the peak sediment load and slightly after when geomorphic changes in the river were at their maximum (in Spring 2013, as reported by East et al. (2018)), resulting in wide, shallow, braided channels and meters of bed aggradation (East et al., 2018). By 2017 the river had begun to incise into its new deposits (East et al., 2018) and appeared to be in dynamic equilibrium with regard to wood storage and export. This is apparently consistent with wood mobilization studies that report total storage of large wood may remain nearly constant (Marcus et al., 2002; van der Nat et al., 2003; Wohl and Goode, 2008; Wohl and Scamardo, 2021; Wohl and Iskin, 2022). However, there was an increase in sediment deposition beyond the wood plateau, up until 2016/17 (Figure 8d), which suggests that sediment bars continued to expand in areal extent, helped at least in part by an up to four-fold increase in wood deposition over a short period of time. This observation is consistent with studies demonstrating sediment transport suppression and sediment deposition through increased hydraulic

roughness due to the introduction of large wood (e.g., Davidson and Eaton, 2013; Wohl, 2017). Large wood covered up to 25% of the available area at the local sub-reach scale, almost always accumulating on top of sediment that otherwise would be available for transport by flows. Further, the largest and most persistent wood accumulations in both reaches are strongly associated with larger braid plains where the river has multiple channels. This is consistent with the observation of Scott and Wohl (2018) in a Pacific Northwest river that wood jams are significantly more likely in deeper and multithreaded channels than shallow and single threaded channels. There is some evidence that a very small portion of wood undergoes at least temporary burial by sediment, from visual evidence of wood appearing partially buried. However, such instances are very rare, and model detection is variable for these partially buried pieces, so we attribute the contribution of such wood to total area as within the 15% reported error. The transition probabilities from wood to sediment constitute 13 and 12% of transitions to sediment in the middle and lower reaches, respectively. These numbers reflect both cases of true burial of wood by sediment, as well the transportation of wood away, exposing sediment. A follow-up study could specifically examine whether sediment deposition was enhanced by the presence of wood, or due to different transport and deposition timescales.

Our measurements provide an integration of both logjams and individual wood pieces, such that we cannot separately report the abundances of each sub-population. However, our remote-sensing observations suggest that the size distributions for wood depositions varied considerably in time and space (Figure 11). The most notable finding was an initial increase in average wood-deposit size coincident with the initial sediment pulse, especially in the middle reach, which was followed by a transition toward smaller deposits. These findings are broadly consistent with those of DeMott (2021), whose dataset consists of six aerial surveys over the middle reach. They note that the sum of logjam area values increased steadily until 2016/17. Additionally, they note that the number of individual logs, a quantity not measured here, spiked in summer 2013 and then fell back down to pre-dam levels. We observe the same initial increase in wood (Figure 9a) that is consistent with the delivery of a pulse of individual logs from the reservoir (Leung, 2019), as well as coinciding with the peak in sediment load (East et al.

2018).

Wood is known to enhance pool formation (e.g., Stewart et al., 2012; Livers and Wohl, 2021), and the fact that sediment bars continued to expand in areal extent until 2016/17, whereas large wood was deposited mostly before winter 2013, may be due to roughness-induced suppression of sediment transport, as discussed above. Alternatively, our observations may suggest that the supply of wood was extinguished faster than the supply of sediment. Using our measurements, which provide total wood storage but do not include rates on large-wood import or export in either reach, this scenario is more difficult to evaluate, but is also plausible. A large but finite amount of wood would have accumulated in both reservoirs during the dam period and local production of wood would be a function of channel change rates, which slowed after peak rates in 2012-13 (East et al., 2018). In addition, dam removal allowed for renewed wood transport from the upper watershed to the middle and lower reaches, so the source of wood to the study area would be a complex combination of these three supplies. There was significantly more deposition of wood in previously vegetated areas of the middle reach than the lower reach (Figure 14), which provides evidence that channel enlargement may have promoted wood recruitment and deposition. The reservoir population of wood presumably dominated the large-wood signal in the years during and following dam removal, suggesting pulses in phase with the erosion of wood-bearing deposits of sediment within each reservoir. Upper watershed wood supply is largely unknown. That noted, the residence time of wood undergoing active transport is unknown, promoting uncertainty in how long it would take a wood pulse to travel through the system. We see a very broad wood accumulation size distributions (Figure 11), implying a wide spectrum of large-wood disaggregation and transport rates. We see a temporary increase in average wood accumulation size associated with the period of reach-wide wood enrichment (Figure 11d), perhaps suggesting a discrete period of wood concentration into larger jams, followed by disaggregation and dispersal. The peak in wood abundance coincides with the peak in average wood deposit size, perhaps partly due to recruitment of wood from floodplain areas that the river accessed by channel migration during peak geomorphic change rates in early 2013 (East et al., 2018). The four years after dam removal saw an approximate doubling of peak flow (from ~200

m^3/s in 2012 to ~400 m^3/s in 2016; Supplemental Figure S7a), which could have recruited wood to the channel through bank erosion. We also see a large amount of persistence in wood, suggesting that many wood accumulations were persistent through a large range of flow and sediment conditions, but also a large degree of local variability in wood and sediment persistence (Figure S9a). Disentangling the sources of the wood may be possible with the higher-frequency imagery that have been collected but have not been processed into orthoimagery (Figure S1). These data coupled with more detailed analyses may provide further clues to the sources, transport, and fate of wood in the Elwha River.

5.3. Comparison of wood and sediment dynamics in the middle and lower reaches

It is instructive to synthesize the similarities and differences in response to dam removal in the two reaches to inform both dam removal processes in other comparable systems, as well as to inform habitat and restoration studies. In both reaches, all sediment bars underwent a net enlargement because of dam removal, and newly supplied wood almost always deposited on sediment bars rather than on floodplains, riffles, and steep channel margins. Magnitudes in time series of reach-averaged wood and sediment totals were remarkably similar (Figure 8), despite differences in reach length, slope, sinuosity, and timing of dam removal. Additionally, the size distributions of wood accumulations in both reaches showed similarity in exponential form, as well as broad similarities in reach-wide time series of mean wood deposit size (Figure 11). Strong correlations were found between the time- and spatial-series of both wood and sediment in both reaches, as well as time series of those quantities between reaches (Table 4). The values and time series of ratios of sediment to wood in both reaches were similar. Finally, similarities existed in the rates of many processes revealed by an analysis of transition (Figure 14), for example, sediment erosion and deposition rates, vegetation burial, and wood deposition. We attribute these similarities to the magnitude of shared upstream flow and sediment boundary condition during peak sediment load which saw similar geomorphic processes simultaneously occur in both reaches (East et

al., 2018), aided by similar distributions of sediment grain size in both reaches (Draut and Ritchie, 2015) and relatively steep slopes.

However, noteworthy differences were also revealed in the response of the two reaches to dam removal. Net increases of wood over the study period were slightly greater in the lower reach, whereas net increases in sediment were greater in the middle reach (Figure 8). A potential reason for this is the comparatively steeper slope of the river in the middle reach, implying greater stream power that is expected to increase throughput of sediment and wood, enhance hydraulic roughness, and suppress bar building compared to the less steep lower reach. The middle reach saw a greater increase in average wood deposit size (Figure 11), which may have further locally increased channel roughness and promoted sediment deposition. While present, this signal in the lower reach was more muted, despite the existence of ELJs in this reach, perhaps due to less flow convergence and accumulation in areas of large-wood accumulations, or less dispersed wood available to source wood pile growth during the time of maximum flows.

Wood in the middle reach was more persistent overall (Figure 14), but persistence was also highly localized (Supplemental Figure S9). Sediment in the lower reach was less persistent, and persistent wood was spatially more variable in that reach (Figure 14). We attribute the relative persistence of wood in the middle reach to many of the initial deposits being formed at relatively high elevation, under elevated flows and sediment loads of the initial period up to winter 2013 when most of the new wood from upstream was deposited. A significant amount of this wood is in the middle portion of the middle reach, whereas most large wood in the lower reach is closer to the river outlet and its persistence lower due to more propensity for wood transport over the generally flatter, lower elevation bars with a larger range of stages for a given flow discharge range.

5.4. Potential benefits of reach-wide pixel-wise measurements for large-wood science, and future work

Reflecting on 50 years of large-wood research, Swanson et al. (2021) concluded that *"Given the documented differences in large wood dynamics across different portions of a river network and between networks in diverse geographic regions, our understanding of large wood in rivers would benefit greatly from coordinated, longterm field studies in multiple field sites that focus on a few key questions. This type of research programme could foster direct comparisons among sites."* Automated measurements of large wood, such as presented here, could arguably make that goal more likely. Our approach to image segmentation using deep learning could likely scale to other similar river systems and similar imagery. The prospect of developing accessible DL-based image segmentation models that may transfer outside of their training contexts, i.e., a specific location, image source, or thematic context, is a potentially significant development for riverine wood science. We therefore intend for our open-source image segmentation software (Buscombe and Goldstein, 2022) and publicly available models (Buscombe, 2023a) and datasets (Buscombe, 2023b) to stimulate further application and research into simultaneous large-wood dynamics in several catchments, as well as to facilitate further research on the Elwha River. This methodology could be used to quantify all wood visible at the surface, especially useful in relatively inaccessible rivers and parts of river systems. Capturing wood over all spatial scales provides an opportunity to examine the role of spatial dispersal in wood transport, formation of jams, trapping efficiency (Wohl et al. 2018), as well as any mophodynamic role of wood that is variously dispersed, in the formation of bars and islands (Piégay 1993; Gurnell et al., 2019).

Because reach-wide pixel-wise measurements facilitate comparison of wood and sediment storage at any scale or location, routine monitoring of large wood at large scale could become an important component of characterizing the natural wood regime of a river. It could prove useful in planning and implementing the removal and construction of structures such as dams and fish passage and establishing the target wood regime for that river (Wohl et al., 2019a). Once monitoring protocols are established, we can continue to learn about the natural recruitment and dynamics of wood in situ, through refining techniques to detect incremental change, as well as adequately capturing catastrophic disturbances that are associated with abrupt increases in mobilized large

wood, such as dam removal or landslides (Ruiz-Villanueva et al., 2014). This approach does not provide useful information on buried large wood, or wood obscured by canopy, unless a high-frequency dataset is used that captures these processes as they happen, but each orthoimage can provide a near-complete synoptic survey of large wood. In the future, addressing any wood load bias due to seasonal or permanent canopy may be achieved using in situ measurements. The extent to which specific large-wood dynamics can be elucidated from the time series depends on the specifics of the undergoing changes and how that intersects with the timing or return interval of the imagery.

Our techniques and insights were not able to compute the magnitude of individual small wood pieces (e.g., Hortobágyi et al., 2024) that were not visible in the 0.125m-resolution imagery, nor were they able to provide volumetric estimates of large wood. Future work could address finer individual wood pieces with higher-resolution imagery, and reach-wide estimates of wood height and porosity could be made to better estimate wood volumes.

In this study, the focus was on how to effectively find and map wood, sediment, and other quantities of interest in imagery of the river corridor, resulting in measurements that were used to quantify wood and sediment at entire catchment scales. As such, and as discussed in section 3.6, the small possible variation in stage-discharge relation during the measurement period does not impact our error analyses or findings. Specifically, we find our automated measurements to be within 15% of the ground truth measurement, and since both measurements use the same imagery, there remains a small possible bias that could be addressed with future work, using a stage-discharge relation. Owing to the propagating nature of the sediment wave, variable amounts of braiding, and variable barface slopes, in order to construct a time-varying hypsometry or stage-discharge relation would have required field measurements of water surface elevations throughout both reaches. This information is unfortunately not available but could be obtained in a future study.

With these potential limitations noted, our measurements, and specifically our deep learning models, may be useful for studying the morphodynamics of wood-sediment interactions in other geomorphically complex channels. For example, Scott and Wohl

(2018) noted that residence times (persistence) remains a major knowledge gap in mountainous watersheds, and Wohl (2020) noted that more knowledge about deposition modes in individual systems would help local wood restoration strategies. Dispersed pieces are assumed to be more mobile, and the distribution among dispersed and concentrated pieces in the large-wood population exchanged between active and stored subpopulations is, at present, largely unknown. The conversion rate between mobile and stored wood populations, assuming there is a sub-population of mobile wood that gets trapped by stored wood (Gurnell et al., 2000) is also not generally known or parameterized. However, techniques like those presented here could in theory be used to identify and track individual pieces or accumulations of large wood, but we argue that would be more effective from a very high-resolution time series of imagery (that is, at a higher resolution than the present study), for example, weekly or monthly resolution, and compute the magnitudes of the mobile and stored sub-populations. Finally, perhaps soon it will be possible to infer more large-wood characteristics using automated methods, for example, the complexity of individual pieces, or classifying wood by age (to infer wood recruitment and the effect of transport processes, among numerous potential uses).

The magnitude of wood stored is the balance between inputs and outputs. Closing a large-wood budget for a river system (Benda and Sias 2003; Lucía et al. 2015; Comiti et al. 2016) requires accurate measurements of inputs (wood arriving from upstream and local areas), and outputs (in this case, wood exiting to sea) (Boivin et al., 2017). Alternatively, our measurements of wood occurrence in each pixel in a time series of maps allow us to measure the storage term of the budget directly.

The use of data like these in future work to map the orientation and other potentially important characteristics of large-wood deposits, and to infer processes at reach scales, would be beneficial. In a study conducted in the channel occupying the former reservoir and immediate downstream, Leung et al. (2019) concluded that the primary control on fluvial scour hole size is the presence or absence of roots, with scour pool volume increasing with root cross-sectional area. The shape and orientation of large-wood deposits were found to have additional effects on scour pool depth, volume, and shape.

In contrast, variability in flow discharge was found to be a control on scour-pool size. While our measurements are limited by a lack of volumetric information about large-wood deposits, further studies could potentially examine these conclusions further using our methods and data to measure the shape and orientation of wood accumulations, and it would also be possible to manually identify larger root wads. Preferential wood orientation occurs during the transport of a large wood, with the rootwad positioned upstream and the trunk pointed in the flow direction. (Abbe and Montgomery, 2003; Davidson and Eaton, 2015). Leung et al. (2019) confirmed this phenomenon in the Elwha River. Therefore, a time series of wood orientation measurements at individual locations in the Elwha River system may reveal the chronology of wood deposition with respect to flow fluctuations or might even be helpful in developing stage-discharge relations if the elevations of recently deposited wood can be mapped.

A spatially comprehensive approach would also allow for assessment of spatial-temporal factors such as the so-called "mode" of wood stored within the river corridor, which may be either dispersed (i.e., individual logs) or concentrated (i.e., logjams) (e.g., Kraft et al. 2011). The mode of stored wood may vary considerably over spatial scales (Abbe and Montgomery 2003, Scott and Wohl 2018) and is related to recruitment and transportation processes (Wohl et al., 2019a; Wohl et al., 2023).

6. Conclusions

We developed new deep-learning methods to provide for fully automated planform measurements of large wood, sediment, vegetation, and water from a time series of whole-river-corridor, decimeter-scale orthoimagery. Our measurements in the Elwha River corridor over multiple years and tens of kilometers are accurate to within 15% and provide an unprecedented level of detail describing the evolution of large wood in the system. These measurements and data could be used further to understand the role of large wood in the processes that cause geomorphic change in this and other alluvial river channels.

Large-wood deposition increased between the start of dam removal (2011) and winter 2013, then plateaued. Sediment bars continued to grow up until 2016/17, assisted by a partially static wood framework deposited predominantly during the period up to winter 2014/15. Large wood typically covered ~5% of the channel margin area, although the largest wood accumulations could cover up to 25% of the available area at the local sub-reach scale. Mean wood accumulation area varied more than three-fold over the study period, increasing rapidly until its peak in summer 2013 and decreasing slowly thereafter. Transitions to/from wood account for up to 21% of all transitions, underlining the importance of wood in this dynamic system.

While the time series of wood and sediment in both reaches are similar in magnitude, the lower reach saw greater net increases in wood, whereas the middle reach saw greater net increases in sediment. The total area of both large wood and sediment as a function of distance along the river were highly correlated. The same was true of time series of wood and sediment in both reaches, and correlations between middle- and lower-reach time series of wood and sediment were also high, suggesting a first-order control on large wood and sediment due to upstream hydrology and wood and sediment supply. An increase in wood in the lower reach, despite the destruction of several engineered logjams during dam removal and subsequent channel adjustment, has likely increased salmon habitat through pool scouring and bar building.

These results not only provide evidence of the substantial changes to the areal distribution of floodplain wood and sediment resulting from dam removal, but also provide evidence that these wood-related changes varied spatially over the study area reaches and subreaches. While novel, these observations and the understanding gained from them may be expanded with the future processing and release of dozens more aerial surveys of the Elwha River that will fill gaps and expand the time-series data.

Future application of these methods has the potential to advance the incomplete theoretical understanding of the dynamics of wood in rivers, such that improvements are made in our abilities to predict the two-way feedbacks of water, sediment, wood, vegetation, and the evolving channel morphology (Swanson et al., 2021). These advances may be possible because of measurements of large wood over meaningful

scales are now possible with deep learning techniques such as those shown here. Automation through remote sensing and deep learning is no substitute for field insight, accuracy, or precision, however, and vegetation canopy and volumetric measurements of wood will remain challenging from aerial orthoimagery alone. Thus, hybrid approaches of remote sensing and field observations continue to be necessary. Automation does provide the benefits of near complete coverage and consistent measurements over any scale. In the future, Machine Learning has potentially limitless application in the science of large wood if detailed field-based and/or multi-modal measurements of wood characteristics can be paired with coincident data such as imagery and high-resolution digital elevation products, to produce models that can identify specific features of interest over large scales.

In conclusion, our approach to evaluating wood dynamics in rivers using remote sensing and image segmentation using deep learning has been designed to scale to other similar river systems with similar imagery. We therefore hope our open-source image segmentation software, publicly available models, and datasets will stimulate further application and research into simultaneous large-wood dynamics in other river catchments, as well as to facilitate further research on the morphodynamics and environmental restoration of the Elwha River.

Open Research

Image segmentation models are available from Buscombe (2023a), which works with the workflows detailed by Buscombe and Goldstein (2022). All data are publicly and freely available in Ritchie et al. (2018) and Buscombe (2023b), except the time-series measurements of alluvial bars in the lower reach made by the Lower Elwha Klallam Tribe.

Acknowledgments

This work was funded by the USGS Coastal and Marine Hazards and Resources Program through the Landscape Response to Disturbance and Remote Sensing Coastal Change projects. The authors would like to thank the Open Source Geospatial Foundation (OSGeo) for providing and maintaining Geospatial Data Abstract Library (GDAL), and for the open-source Keras (https://keras.io) community, maintaining a deep-learning API written in Python, running on top of the machine-learning platform Tensorflow. Without these software tools this work would be impossible. We are also grateful to Sharon Fitzpatrick and Jaycee Favela for their contribution to image labeling, and to Tim Abbe for valuable comments. Thanks to Chris Sherwood, Peter Swarzenski, Chris Magirl, and two anonymous reviewers for their valuable feedback. Thanks to Mel Elofson, Earnest Sampson and mcKenzi Taylor for collecting Tribal engineered log jam data. Any use of trade, firm, or product names is for descriptive purposes only and does not imply endorsement by the U.S. Government

References

Abbe, T.B., & Montgomery, D.R. (1996). Large woody debris jams, channel hydraulics and habitat formation in large rivers. *Regulated Rivers: Research and Management,* 12, 201–221.

Abbe, T., Montgomery, D.R., & Petroff, C. (1997). *Design of Stable In-Channel Wood Debris Structures for Bank Protection and Habitat Restoration: An Example from the Cowlitz River, WA*. 809-816 in: S.S.Y. Wang, E.J. Langendoen, and F.D. Shields Jr. (eds.), Proceedings of the Conference on Management of Landscapes Disturbed by Channel Incision. University of Mississippi, University, Mississippi.

Abbe, T.B., Brooks, A.P., & Montgomery, D.R. (2003). *Wood in river rehabilitation and management*, in: Gregory, S.V., Boyer, K.L., & Gurnell, A.M. (Eds.), The Ecology and Management of Wood in World Rivers. American Fisheries Society, Bethesda, Maryland, 367–389.

Abbe, T., & Brooks, A. (2011). *Geomorphic, engineering, and ecological considerations when using wood in river restoration*. In: Stream restoration in dynamic fluvial systems: Scientific approaches, analyses, and tools, *194*, 419–451.

Abbe T.B., & Montgomery D.R. (2003). Patterns and processes of wood debris accumulation in the Queets River basin, Washington. *Geomorphology,* 51, 81–107.

Aleissaee, A.A., Kumar, A., Anwer, R.M., Khan, S., Cholakkal, H., Xia, G.S., & Khan, F.S. (2023). Transformers in remote sensing: A survey. *Remote Sensing*, *15*(7), 1860.

Atha, J.B. (2014). Identification of fluvial wood using Google Earth. *River Research and Applications*, 30(7), 857-864.

Atha, J.B., & Dietrich, J.T. (2016). Detecting fluvial wood in forested watersheds using LiDAR data: a methodological assessment. *River Research and Applications*, 32(7), 1587-1596.

Beechie, T.J., Liermann, M., Pollock, M.M., Baker, S., & Davies, J. (2006). Channel pattern and river-floodplain dynamics in forested mountain river systems. *Geomorphology,* 78, 124–141.

Benda L.E., & Sias, J.C. (2003). A quantitative framework for evaluating the mass balance of in-stream organic debris. *Forest Ecology and Management,* 172, 1–16.

Bertoldi, W., Gurnell, A.M., & Welber, M. (2013). Wood recruitment and retention: the fate of eroded trees on a braided river explored using a combination of field and remotely-sensed data sources. *Geomorphology*, 180–181, 146–155.

Boivin M, Buffin-Belanger T, & Piegay, H. (2015). The raft of the Saint-Jean River, Gaspé (Québec, Canada): A dynamic feature trapping most of the wood transported from the catchment. *Geomorphology,* 231, 270–280.

Boivin, M., Buffin-Bélanger, T. & Piégay, H., (2017). Estimation of large wood budgets in a watershed and river corridor at interdecadal to interannual scales in a cold-temperate fluvial system. *Earth Surface Processes and Landforms*, *42*(13), 2199-2213.

Bountry, J. A., Randle, T. J., & Ritchie, A. (2018). Adaptive sediment management program final report for the Elwha River restoration project. U.S. Bureau of Reclamation, Technical Report SRH-2018-13 (276 pp.).

Buscombe, D. (2023a). Doodleverse/Segmentation Gym SegFormer models for 4-class (other, water, sediment, wood) segmentation of RGB aerial orthomosaic imagery (v1.0) [Data set]. *Zenodo*. https://doi.org/10.5281/zenodo.8172858

Buscombe, D. (2023b). Labeled high-resolution orthoimagery time-series of an alluvial river corridor; Elwha River, Washington, USA. (1.0) [Data set]. *Zenodo*. https://doi.org/10.5281/zenodo.10155783

Buscombe, D., & Goldstein, E. B. (2022). A reproducible and reusable pipeline for segmentation of geoscientific imagery. *Earth and Space Science*, 9, e2022EA002332.

Buscombe, D., Goldstein, E. B., Sherwood, C. R., Bodine, C., Brown, J. A., Favela, J., et al. (2021). Human-in-the-loop segmentation of Earth surface imagery. *Earth and Space Science*, 9, e2021EA002085.

Campbell, J.L., Green, M.B., Yanai, R.D., Woodall, C.W., Fraver, S., Harmon, M.E., et al. (2019). Estimating uncertainty in the volume and carbon storage of downed coarse woody debris. *Ecological Applications,* 29(2), e01844.

Collins, B.D., Montgomery, D.R., & Haas, A.D. (2002). Historical changes in the distribution and functions of large wood in Puget Lowland rivers. *Canadian Journal of Fisheries and Aquatic Sciences*, *59*(1), 66–76.

Collins, B.D., Montgomery, D.R., Fetherston, K.L., & Abbe, T.B. (2012). The floodplain large-wood cycle hypothesis: a mechanism for the physical and biotic structuring of temperate forested alluvial valleys in the North Pacific coastal ecoregion. *Geomorphology* 139–140: 460–470.

Comiti, F., Andreoli, A., Mao, L., & Lenzi, M.A. (2008). Wood storage in three mountain streams of the Southern Andes and its hydro-morphological effects. *Earth Surface Processes and Landforms 33*(2), pp.244-262.

Comiti, F., Lucía, A., & Rickenmann, D. (2016). Large wood recruitment and transport during large floods: A review. *Geomorphology,* 269, 23–39

Davidson, S.L., & Eaton, B.C. (2013). Modeling channel morphodynamic response to variations in large wood: Implications for stream rehabilitation in degraded watersheds. *Geomorphology,* 202, 59–73. https://doi.org/10.1016/j.geomorph.2012.10.005

Davidson, S.L., & Eaton, B.C. (2015). Simulating riparian disturbance: Reach scale impacts on aquatic habitat in gravel bed streams. *Water Resources Research*, *51*(9), 7590-7607.

Davis, J.C., & Sampson, R.J. (1986). *Statistics and Data Analysis in Geology* (Vol. 646). New York: Wiley.

DeMott, A.D. (2021). Long-term Geomorphic Effects of the Glines Canyon Dam Removal on the Elwha River, Washington, USA". *Central Washington University Master's Thesis*. https://digitalcommons.cwu.edu/etd/1506

Draut, A.E., & Ritchie, A.C. (2015). Sedimentology of new fluvial deposits on the Elwha River, Washington, USA, formed during large-scale dam removal. *River Research and Applications*, *31*(1), 42–61.

Draut, A.E., Logan, J.B., & Mastin, M.C. (2011). Channel evolution on the dammed Elwha River, Washington, USA. *Geomorphology,* 127, 71–87.

Duda, J.J., Freilich, J.E., & Schreiner, E.G. (2008). Baseline studies in the Elwha River ecosystem prior to dam removal: Introduction to the special issue. *Northwest Science*, *82*, 1–12.

Duchon, C.E. (1979). Lanczos filtering in one and two dimensions. *Journal of Applied Meteorology and Climatology*, 18(8), 1016-1022.

East, A.E., Pess, G.R., Bountry, J.A., Magirl, C.S., Ritchie, A.C., Logan, J., et al. (2015). Large-scale dam removal on the Elwha River, Washington, USA: River channel and floodplain geomorphic change. *Geomorphology*, *228*, 765–786.

East, A.E., Logan, J.B., Mastin, M.C., Ritchie, A.C., Bountry, J.A., Magirl, C.S. & Sankey, J.B. (2018). Geomorphic evolution of a gravel-bed river under sediment-starved versus sediment-rich conditions: River response to the world's largest dam removal. *Journal of Geophysical Research: Earth Surface*, *123*(12), 3338–3369.

Fetherston, K.L., Naiman, R.J., & Bilby, R.E. (1995). Large woody debris, physical processes, and riparian forest development in montane river networks of the Pacific Northwest. *Geomorphology*, 13, 133–144.

Fieberg, J., & Ellner, S.P. (2001). Stochastic matrix models for conservation and management: a comparative review of methods. *Ecology Letters*, *4*(3), 244-266.

Frissell, C.A., Liss, W.J., Warren, C.E. & Hurley, M.D. (1986). A hierarchical framework for stream habitat classification: viewing streams in a watershed context. *Environmental Management*, *10*, 199-214.

Grabowski, R.C., Gurnell, A.M., Burgess-Gamble, L., England, J., Holland, D., Klaar, M.J., et al. (2019). The current state of the use of large wood in river restoration and management. *Water and Environment Journal*, *33*(3), 366-377.

Grabowski, J., & Wohl, E. (2021). Logjam attenuation of annual sediment waves in eolian-fluvial environments, North Park, Colorado, USA. *Geomorphology,* 375, 107494.

Gurnell, A.M., Bertoldi, W., Francis, R.A., Gurnell, J., & Mardhiah, U. (2019). Understanding processes of island development on an island braided river over timescales from days to decades. *Earth Surface Processes and Landforms*, *44*(2), 624-640.

Gurnell, A.M., Petts, G.E., Hannah, D.M., Smith, B.P., Edwards, P.J., Kollmann, J., et al. (2000). Wood storage within the active zone of a large European gravel-bed river. *Geomorphology*, *34*(1-2), pp.55-72.

Gurnell, A.M., Piégay, H., Swanson, F.J., & Gregory, S.V. (2002). Large wood and fluvial processes. *Freshwater Biology*, *47*(4), 601-619.

Haschenburger, J.K., & Rice, S.P. (2004). Changes in woody debris and bed material texture in a gravel-bed channel. *Geomorphology*, 60(3-4), 241-267.

Hortobágyi, B., Petit, S., Marteau, B., Melun, G. and Piégay, H., 2024. A high-resolution inter-annual framework for exploring hydrological drivers of large wood dynamics. River Research and Applications.

Iroumé, A., Sánchez, K., Mazzorana, B., Martini, L. & Picco, L. (2023). Large wood dynamics in a mountain river disturbed by a volcanic eruption. *Geomorphology*, 422, 108551.

Kasprak, A., Magilligan, F.J., Nislow, K.H., & Snyder, N.P. (2012). A Lidar-derived evaluation of watershed-scale large woody debris sources and recruitment mechanisms: Coastal Maine, USA. *River Research and Applications*, 28(9), 1462-1476.

Kentsch, S., Lopez Caceres, M.L., Serrano, D., Roure, F., & Diez, Y. (2020). Computer vision and deep learning techniques for the analysis of drone-acquired forest images, a transfer learning study. *Remote Sensing*, *12*(8), 1287.

Khan, S., Naseer, M., Hayat, M., Zamir, S.W., Khan, F.S., & Shah, M. (2022). Transformers in vision: A survey. *ACM computing surveys (CSUR)*, *54*, 1-41.

Kraft, C.E., Warren, D.R., & Keeton, W.S. (2011). Identifying the spatial pattern of wood distribution in northeastern North American streams. *Geomorphology,* 135, 1–7.

Kramer, N., Wohl, E., Hess-Homeier, B. & Leisz, S. (2017). The pulse of driftwood export from a very large forested river basin over multiple time scales, Slave River, Canada. *Water Resources Research*, *53*(3), 1928-1947.

Kuiper, S.D., Coops, N.C., Jarron, L.R., Tompalski, P. & White, J.C. (2023). An automated approach to detecting instream wood using airborne laser scanning in small coastal streams. *International Journal of Applied Earth Observation and Geoinformation*, 118, 103272.

Lassettre, N.S., Piégay, H., Dufour, S. & Rollet, A.J. (2008). Decadal changes in distribution and frequency of wood in a free meandering river, the Ain River, France. *Earth Surface Processes and Landforms*, *33*(7), 1098-1112.

Latterell, J. J., Bechtold, J. S., O'Keefe, T. C., & Naiman, R. J. (2008). Dynamic patch mosaics and channel movement in an unconfined river valley of the Olympic Mountains. *Freshwater Biology,* 51, 523–544.

Linardatos, P., Papastefanopoulos, V., & Kotsiantis, S. (2020). Explainable AI: A review of machine learning interpretability methods. *Entropy*, *23*(1), 18.

Livers, B., Lininger, K.B., Kramer, N., & Sendrowski, A. (2020). Porosity problems: Comparing and reviewing methods for estimating porosity and volume of wood jams in the field. *Earth Surface Processes and Landforms*, 45(13), 3336-3353.

Livers, B., & Wohl, E. (2021). All logjams are not created equal. *Journal of Geophysical Research: Earth Surface,* 126, e2021JF006076.

Long, J., Shelhamer, E., & Darrell, T. (2015). Fully convolutional networks for semantic segmentation. In *Proceedings of the IEEE Conference on Computer Vision and Pattern Recognition,* 3431-3440.

Lucía, A., Comiti, F., Borga, M., Cavalli, M., & Marchi, L. (2015). Dynamics of large wood during a flash flood in two mountain catchments. *Natural Hazards and Earth System Sciences,* 3, 1643–1680.

Leung, V. (2019). *Large woody debris and river morphology in scour pool formation, dam removal, and delta formation*. University of Washington doctoral dissertation https://digital.lib.washington.edu/researchworks/handle/1773/45030

Major, J.J., East, A.E., O'Connor, J.E., Grant, G.E., Wilcox, A.C., Magirl, C.S., et al. (2017). Geomorphic responses to dam removal in the United States–a two-decade perspective. *Gravel-bed rivers: Processes and disasters*, 355-383.

Marcus, W.A., Marston, R.A., Colvard Jr, C.R., & Gray, R.D. (2002). Mapping the spatial and temporal distributions of woody debris in streams of the Greater Yellowstone Ecosystem, USA. *Geomorphology*, 44(3-4), 323-335.

Massong T.M., & Montgomery D.R. (2000). Influence of sediment supply, lithology, and wood debris on the distribution of bedrock and alluvial channels. *Geological Society of America Bulletin,* 112, 591–599.

Matthews, B.W. (1975). Comparison of the predicted and observed secondary structure of T4 phage lysozyme. *Biochimica et Biophysica Acta (BBA)-Protein Structure*, *405*(2), 442-451.

Maxwell, A.E., Warner, T.A., & Guillén, L.A. (2021). Accuracy assessment in convolutional neural network-based deep learning remote sensing studies—Part 1: Literature review. *Remote Sensing*, *13*(13), 2450.

McDowell, C., & Hassan, M. (2024). Response of a small, forested stream to a large input of sediment. *Geomorphology*, 447, 109002.

McHenry, M.L., Shott, E., Conrad, R.H. and Grette, G.B., 1998. Changes in the quantity and characteristics of large woody debris in streams of the Olympic Peninsula, Washington, USA (1982-1993). *Canadian Journal of Fisheries and Aquatic Sciences*, *55*(6), pp.1395-1407.

McHenry, M., Pess, G., Abbe, T., Coe, H., Goldsmith, J., Liermann, M., et al. (2007). The physical and biological effects of engineered log jams (ELJs) in the Elwha River, Washington. *Report to Washington State Salmon Recovery Board and Interagency Committee of Outdoor Recreation (IAC)*. 90 pages. http://www.fws.gov/wafwo/fisheries/Publications/Elwha%20ELJ%20Monitoring%20Final%20Reportfinal.pdf

Montgomery, D.R., Abbe, T.B., Buffington, J.M., Peterson, N.P., Schmidt, K.M., & Stock, J.D. (1996). Distribution of bedrock and alluvial channels in forested mountain drainage basins. *Nature,* 381, 587-589

Moulin, B., & Piégay, H. (2004). Characteristics and temporal variability of large woody debris trapped in a reservoir on the River Rhone (Rhone): Implications for river basin management. *River Research and Applications*, *20*(1), 79-97.

Nagayama, S., & Nakamura, F. (2010). Fish habitat rehabilitation using wood in the world. *Landscape and Ecological Engineering,* 6, 289–305.

Nanson, G.C., Barbetti, M., & Taylor, G. (1995). River stabilisation due to changing climate and vegetation during the late Quaternary in western Tasmania, Australia. *Geomorphology,* 13, 145–158.

Ortega-Terol, D., Moreno, M.A., Hernández-López, D., & Rodríguez-Gonzálvez, P. (2014). Survey and classification of large woody debris (LWD) in streams using generated low-cost geomatic products. *Remote Sensing*, *6*(12), 11770-11790.

Over, J.R., Ritchie, A.C., Kranenburg, C.J., Brown, J.A., Buscombe, D., Noble, T., et al. (2021). Processing coastal imagery with Agisoft Metashape Professional Edition, version 1.6—Structure from motion workflow documentation: *U.S. Geological Survey Open-File Report* 2021–1039, 46 p., https://doi.org/10.3133/ofr20211039.

Pearson, A.J., Snyder, N.P., & Collins, M.J. (2011). Rates and processes of channel response to dam removal with a sand-filled impoundment. *Water Resources Research*, *47*(8), W08504.

Pfeiffer, A., & Wohl, E. (2018). Where does wood most effectively enhance storage? Network-scale distribution of sediment and organic matter stored by instream wood. *Geophysical Research Letters,* 45, 194–200.

Pess, G. R., McHenry, M. L., Beechie, T. J., & Davies, J. (2008). Biological impacts of the Elwha River dams and potential salmonid responses to dam removal. *Northwest Science* 82, 72–90.

Pess, G.R., Liermann, M.C., McHenry, M.L., Peters, R.J., & Bennett, T.R. (2012). Juvenile salmon response to the placement of engineered log jams (ELJs) in the Elwha River, Washington State, USA. *River Research and Applications*, *28*(7), 872-881.

Piégay H. (1993). Nature, mass and preferential sites of coarse woody debris deposits in the Lower Ain valley (Mollon reach), France. *Regulated Rivers: Research and Management,* 8, 359–372.

Pohl, M. (2004). Channel bed mobility downstream from the Elwha dams, Washington. *The Professional Geographer*, *56*(3), 422-431.

Ritchie, A.C., Warrick, J.A., East, A.E., Magirl, C.S., Stevens, A.W., Bountry, J.A., et al. (2018a). Morphodynamic evolution following sediment release from the world's largest dam removal. *Scientific Reports*, *8*(1), 13279.

Ritchie, A.C., Curran, C.A., Magirl, C.S., Bountry, J.A., Hilldale, R.C., Randle, T.J., & Duda, J.J. (2018b). Data in support of 5-year sediment budget and morphodynamic analysis of Elwha River following dam removals: *U.S. Geological Survey data release*, https://doi.org/10.5066/F7PG1QWC.

Roni, P., Beechie, T., Pess, G., & Hanson, K. (2015). Wood placement in river restoration: fact, fiction, and future direction. *Canadian Journal of Fisheries and Aquatic Sciences*, *72*(3), 466-478.

Ruiz-Villanueva V., Díez-Herrero A., Ballesteros J.A., & Bodoque J.M. (2014). Potential large woody debris recruitment due to landslides, bank erosion and floods in mountain basins: A quantitative estimation approach. *River Research and Applications,* 30, 81–97.

Ruiz-Villanueva, V., Piégay, H., Gurnell, A.M., Marston, R.A., & Stoffel, M. (2016). Recent advances quantifying the large wood dynamics in river basins: New methods and remaining challenges. *Reviews of Geophysics*, 54(3), 611-652.

Rußwurm, M., & Körner, M. (2020). Self-attention for raw optical satellite time series classification. *ISPRS Journal of Photogrammetry and Remote Sensing*, *169*, 421-435.

Sanhueza, D., Picco, L., Ruiz-Villanueva, V., Iroumé, A., Ulloa, H. & Barrientos, G. (2019). Quantification of fluvial wood using UAVs and structure from motion. *Geomorphology*, 345, 106837.

Sanhueza, D., Picco, L., Paredes, A., & Iroumé, A. (2022). A faster approach to quantify large wood using UAVs. *Drones*, *6*(8), 218.

Schanz, S.A., Montgomery, D.R., Collins, B.D., & Duvall, A.R. (2018). Multiple paths to straths: A review and reassessment of terrace genesis. *Geomorphology*, 312, 12-23.

Scott D.N., & Wohl E. (2018). Natural and anthropogenic controls on wood loads in river corridors of the Rocky, Cascade, and Olympic Mountains, USA. *Water Resources Research* 54, 7893–7909.

Sendrowski, A., & Wohl, E. (2021). Remote sensing of large wood in high-resolution satellite imagery: Design of an automated classification work-flow for multiple wood deposit types. *Earth Surface Processes and Landforms*, 46(12), 2333-2348.

Sendrowski, A., Wohl, E., Hilton, R., Kramer, N., & Ascough, P. (2023). Wood-based carbon storage in the Mackenzie River Delta: The world's largest mapped riverine wood deposit. *Geophysical Research Letters*, 50, e2022GL100913.

Senter, A.E., & Pasternack, G.B. (2011). Large wood aids spawning Chinook salmon (Oncorhynchus tshawytscha) in marginal habitat on a regulated river in California. *River Research and Applications*, *27*(5), 550-565.

Shafroth, P.B., Perry, L.G., Rose, C.A. and Braatne, J.H., 2016. Effects of dams and geomorphic context on riparian forests of the Elwha River, Washington. *Ecosphere*, 7(12), p.e01621

Smikrud, K.M., & Prakash, A. (2006). Monitoring large woody debris dynamics in the Unuk River, Alaska using digital aerial photography. *GIScience & Remote Sensing*, 43(2), 142-154.

Spreitzer, G., Tunnicliffe, J., & Friedrich, H. (2019). Using Structure from Motion photogrammetry to assess large wood (LW) accumulations in the field. *Geomorphology*, *346*, 106851.

Stewart, P.M., Bhattarai, S., Mullen, M.W., Metcalf, C.K., & Reátegui-Zirena, E.G. (2012). Characterization of large wood and its relationship to pool formation and macroinvertebrate

metrics in southeastern coastal plain streams, USA. *Journal of Freshwater Ecology*, *27*(3), 351-365.

Stock, J.D., Montgomery, D.R., Collins, B.D., Dietrich, W.E., & Sklar, L. (2005). Field measurements of incision rates following bedrock exposure: Implications for process controls on the long profiles of valleys cut by rivers and debris flows. *Geological Society of America Bulletin*, 117(1-2), 174-194.

Swanson, F.J., Gregory, S.V., Iroumé, A., Ruiz-Villanueva, V., & Wohl, E. (2021). Reflections on the history of research on large wood in rivers. *Earth Surface Processes and Landforms*, 46(1), 55-66.

Takada, T., Miyamoto, A., & Hasegawa, S.F. (2010). Derivation of a yearly transition probability matrix for land-use dynamics and its applications. *Landscape Ecology*, *25*, 561-572.

Tamminga, A., Hugenholtz, C., Eaton, B., & Lapointe, M. (2015). Hyperspatial remote sensing of channel reach morphology and hydraulic fish habitat using an unmanned aerial vehicle (UAV): A first assessment in the context of river research and management. *River Research and Applications*, 31(3), 379-391.

Tsunetaka, H., Mtibaa, S., Asano, S., Okamoto, T., & Kurokawa, U. (2021). Comparison of length and dynamics of wood pieces in streams covered with coniferous and broadleaf forests mapped using orthophotos acquired by an unmanned aerial vehicle. *Progress in Earth and Planetary Science*, 8, 1-16.

Ulloa, H., Iroumé, A., Mao, L., Andreoli, A., Diez, S., & Lara, L.E. (2015). Use of remote imagery to analyse changes in morphology and longitudinal large wood distribution in the Blanco River after the 2008 Chaitén volcanic eruption, southern Chile. *Geografiska Annaler: Series A, Physical Geography*, 97(3), 523-541.

U.S. Geological Survey, 2023, National Water Information System: U.S. Geological Survey web interface, http://dx.doi.org/10.5066/F7P55KJN. Cited May 2023 at https://nwis.waterdata.usgs.gov/nwis. <or enter that date when you accessed your data>

Vandaele, R., Dance, S.L., & Ojha, V. (2021). Deep learning for automated river-level monitoring through river-camera images: an approach based on water segmentation and transfer learning. *Hydrology and Earth System Sciences*, *25*(8), 4435-4453.

Van der Nat D., Tockner K., Edwards P.J., & Ward J.V. (2003). Large wood dynamics of complex Alpine river floodplains. *Journal of the North American Benthological Society* 22, 35–50.

Vaswani, A., Shazeer, N., Parmar, N., Uszkoreit, J., Jones, L., Gomez, A.N., et al. (2017). Attention is all you need. *Advances in Neural Information Processing Systems*, *30*.

Warren, D.R., & Kraft, C.E. (2008). Dynamics of large wood in an eastern US mountain stream. *Forest Ecology and Management*, 256(4), 808-814.

Warrick, J.A., Bountry, J.A., East, A.E., Magirl, C.S., Randle, T.J., Gelfenbaum, G., et al. (2015). Large-scale dam removal on the Elwha River, Washington, USA: Source-to-sink sediment budget and synthesis. *Geomorphology*, *246*, 729-750.

Warrick, J.A., Draut, A.E., McHenry, M.L., Beirne, M.M., & Logan, J.B. (2011). Geomorphology of the Elwha. *Coastal Habitats of the Elwha River, Washington: Biological and Physical Patterns and Processes Prior to Dam Removal*, p.47.

Warrick, J.A., Ritchie, A.C., Adelman, G., Adelman, K., & Limber, P.W. (2017). New techniques to measure cliff change from historical oblique aerial photographs and structure-from-motion photogrammetry. Journal of Coastal Research, 33(1), 39-55.

Wohl, E. (2011). What should these rivers look like? Historical range of variability and human impacts in the Colorado Front Range, USA. *Earth Surface Processes and Landforms*, *36*(10), 1378-1390.

Wohl, E. (2017). Bridging the gaps: An overview of wood across time and space in diverse rivers. *Geomorphology*, 279, 3–26.

Wohl, E. (2019). Forgotten legacies: understanding and mitigating historical human alterations of river corridors. *Water Resources Research*, *55*(7), 5181-5201.

Wohl, E. (2020). Wood process domains and wood loads on floodplains. *Earth Surface Processes and Landforms*, *45*(1), 144-156.

Wohl, E., Bledsoe, B.P., Fausch, K.D., Kramer, N., Bestgen, K.R., & Gooseff, M.N. (2016). Management of large wood in streams: an overview and proposed framework for hazard evaluation. *JAWRA Journal of the American Water Resources Association*, *52*(2), 315-335.

Wohl, E., Brierley, G., Cadol, D., Coulthard, T.J., Covino, T., Fryirs, K.A., et al. (2019b). Connectivity as an emergent property of geomorphic systems. *Earth Surface Processes and Landforms*, *44*(1), 4-26.

Wohl, E., & Goode, J.R. (2008). Wood dynamics in headwater streams of the Colorado Rocky Mountains. *Water Resources Research*, *44*(9), W09429.

Wohl, E., & Iskin, E.P. (2021). Damming the wood falls. *Science Advances*, *7*(50), eabj0988.

Wohl, E., & Iskin, E.P. (2022). The Transience of Channel-Spanning Logjams in Mountain Streams. *Water Resources Research*, *58*(5), e2021WR031556.

Wohl, E., Kramer, N., Ruiz-Villanueva, V., Scott, D.N., Comiti, F., Gurnell, A.M., et al. (2019a). The natural wood regime in rivers. *BioScience*, *69*(4), 259-273.

Wohl, E., & Scamardo, J.E. (2021). The resilience of logjams to floods. *Hydrological Processes*, *35*(1), e13970.

Wohl E., Scott, D.N., & Lininger, K.B. (2018). Spatial distribution of channel and floodplain large wood in forested river corridors of the Northern Rockies. *Water Resources Research* 54, 7879–7892.

Wohl, E., Scott, D.N., & Lininger, K.B. (2018). Spatial distribution of channel and floodplain large wood in forested river corridors of the Northern Rockies. *Water Resources Research*, *54*(10), 7879-7892.Wohl, E., Uno, H., Dunn, S.B., Kemper, J.T., Marshall, A., Means-Brous, M., et al. (2023). Why wood should move in rivers. *River Research and Applications*, 1–12.

Wohl, E., Uno, H., Dunn, S.B., Kemper, J.T., Marshall, A., Means-Brous, M., Scamardo, J.E. and Triantafillou, S.P., 2024. Why wood should move in rivers. *River Research and Applications*, 40(6), pp.976-987

Xie, E., Wang, W., Yu, Z., Anandkumar, A., Alvarez, J.M., & Luo, P. (2021). SegFormer: Simple and efficient design for semantic segmentation with transformers. *Advances in Neural Information Processing Systems*, 34, 12077-12090.

Zhang, M., Singh, H., Chok, L., & Chunara, R. (2022). Segmenting across places: The need for fair transfer learning with satellite imagery. In *Proceedings of the IEEE/CVF Conference on Computer Vision and Pattern Recognition*, 2916-2925.

Zhou, B., Zhao, H., Puig, X., Xiao, T., Fidler, S., Barriuso, A., and Torralba, A. (2019). Semantic understanding of scenes through the ADE20K dataset. *International Journal of Computer Vision*, *127*, 302-321.

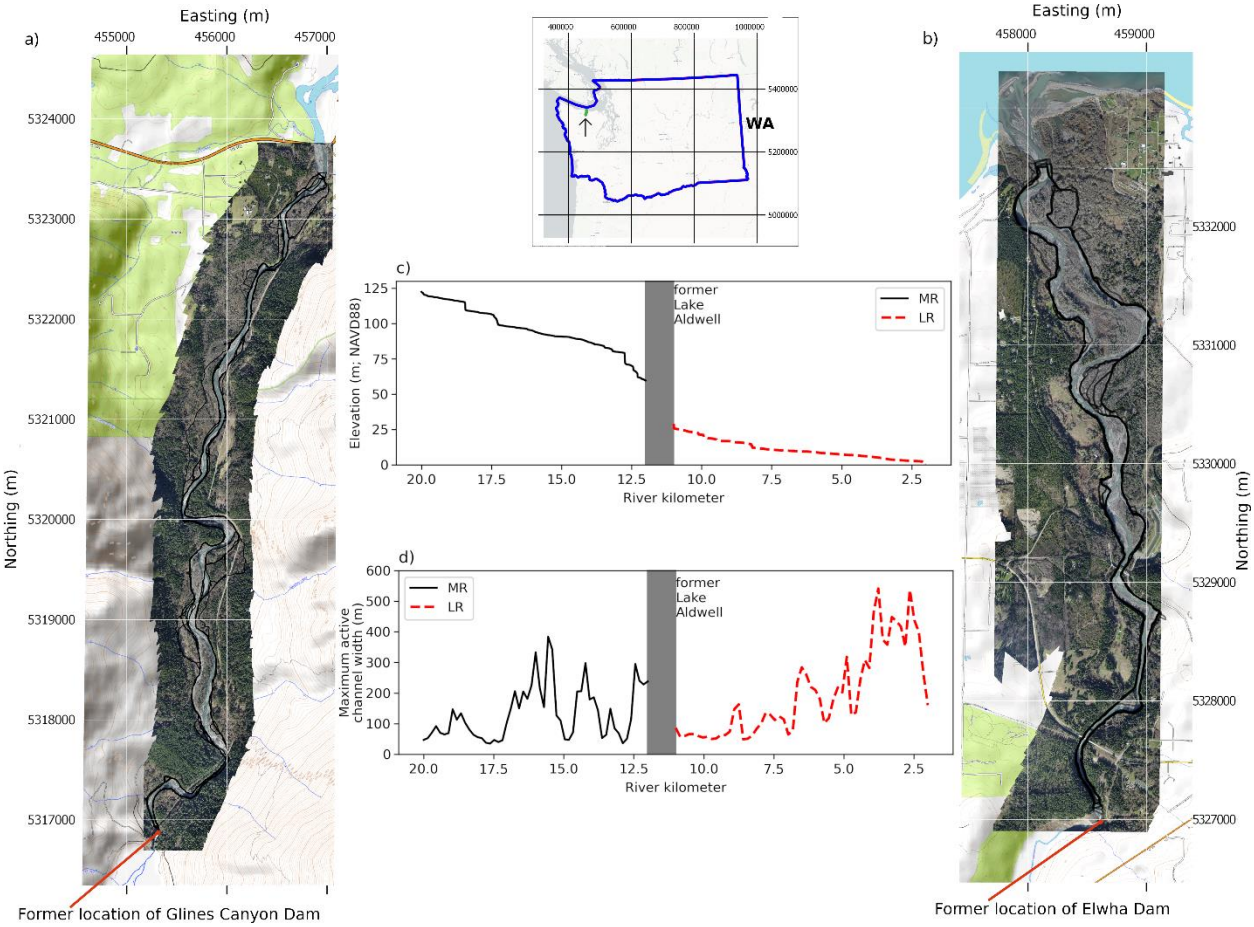

Figure 1: The two reaches of the Elwha River under consideration, namely a) the middle reach (MR) and b) the lower reach (LR), located in the Olympic Peninsula of Washington, USA (inset map) and draining into the Strait of Juan de Fuca in the Salish Sea. The two reaches are illustrated using orthoimagery reconstructed from one aerial flight conducted on 2015-03-03. Imagery comes from Ritchie et al. (2018). The digitized active channel margins are from East et al. (2018). Eastings and Northings are NAD83(2011) UTM 10N. c) The elevation profile of the river. d) The maximum active channel width, determined from the 14-point time series of orthoimagery that spans the study period. USGS streamgage (U.G. Geological

Survey, 2023) 12046260 is located at 48°06'44", 123°33'03". Base maps from https://www.openstreetmap.org/.

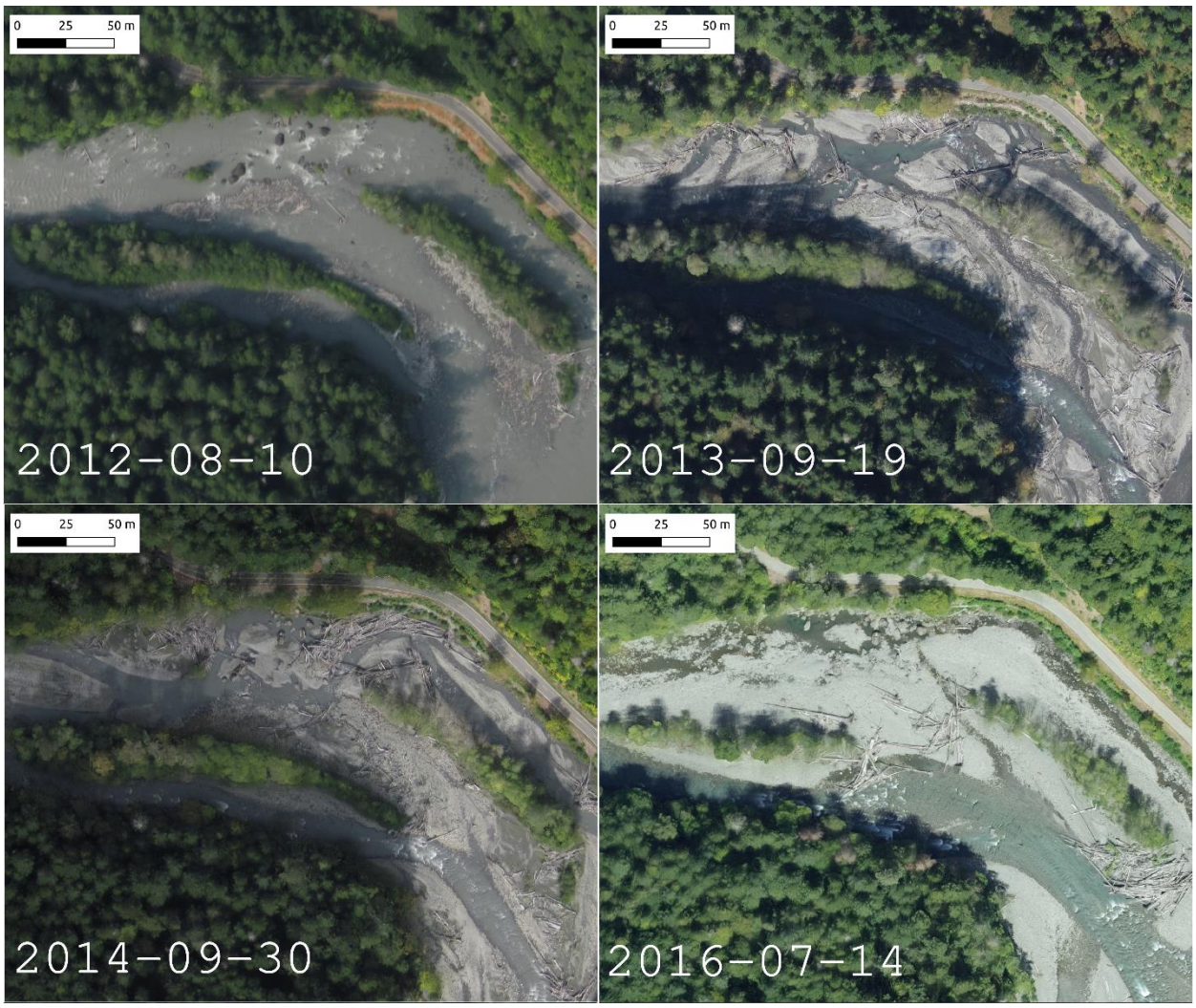

Figure 2: Example orthoimagery at a typical location (located in the middle reach), showing the variation in color and brightness, as well as the nature of the channel, wood deposition, and bar growth. Please see Supplemental Figure S1 for the full 14-image time series of orthoimagery at this location, as well as the variation in average image brightness.

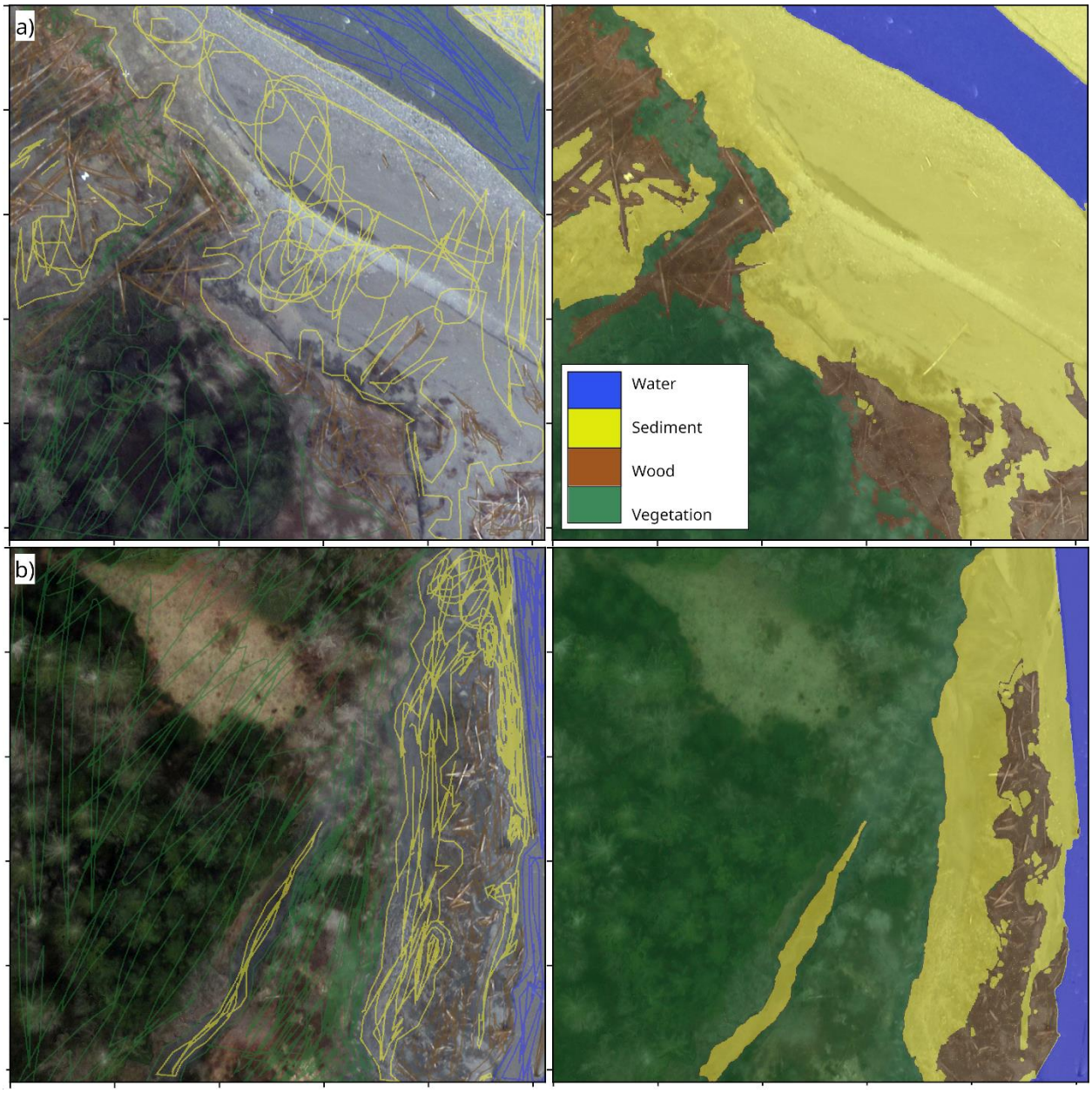

Figure 3: Example annotated images (left column) and resulting label images (right column) made using the software program Doodler (Buscombe et al., 2021). Spacing between ticks is 200 pixels. Please see Supplemental Figure S14 for more examples of annotated imagery and labels.

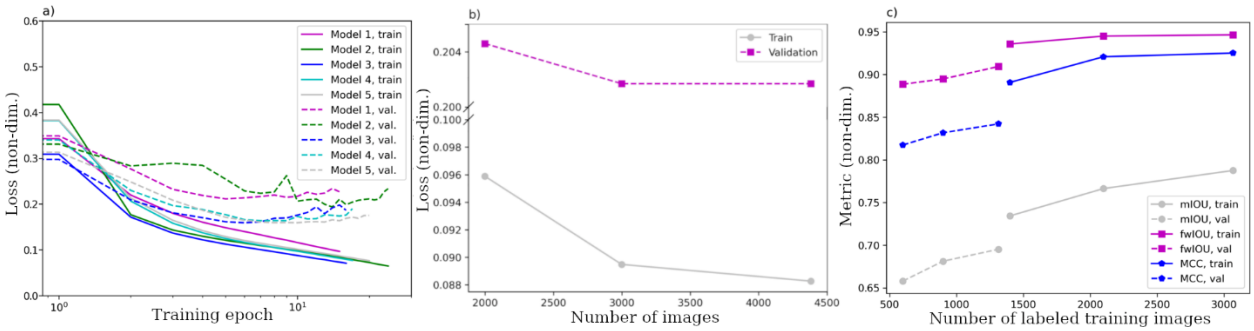

Figure 4: a) Loss curves for additional training runs for the 4-class image segmentation model (b) The minimum train and validation loss from the best four-class model trained with increasing numbers of labeled images. (c) Various train/validation metrics (mean intersection-over-union or IoU, frequency weighted IoU, and Matthew's Correlation Coefficient) as a function of number of training/validation images.

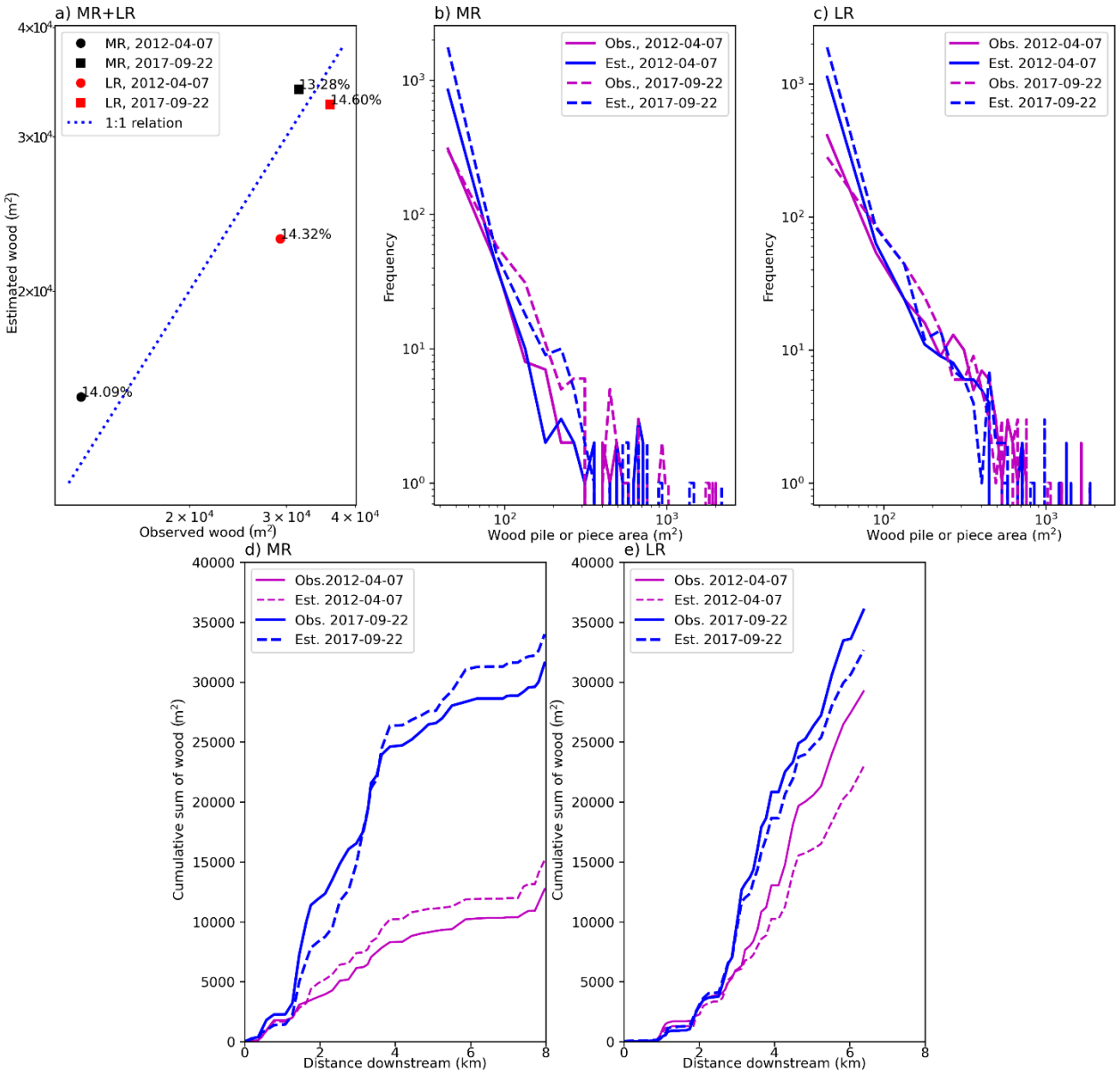

Figure 5: Model wood detection evaluation. Each panel shows results from all four sets of ground truth observations (from lower reach or LR and middle reach or MR, 2012-04-07 and 2017-09-22 respectively). a) Observed versus estimated total wood area; b) Observed and estimated wood deposit size-distributions in the MR; c) Observed and estimated wood deposit size-distributions in the LR; d) Cumulative sum of wood as a function of distance downstream in the MR; and e) Cumulative sum of wood as a function of distance downstream in the LR.

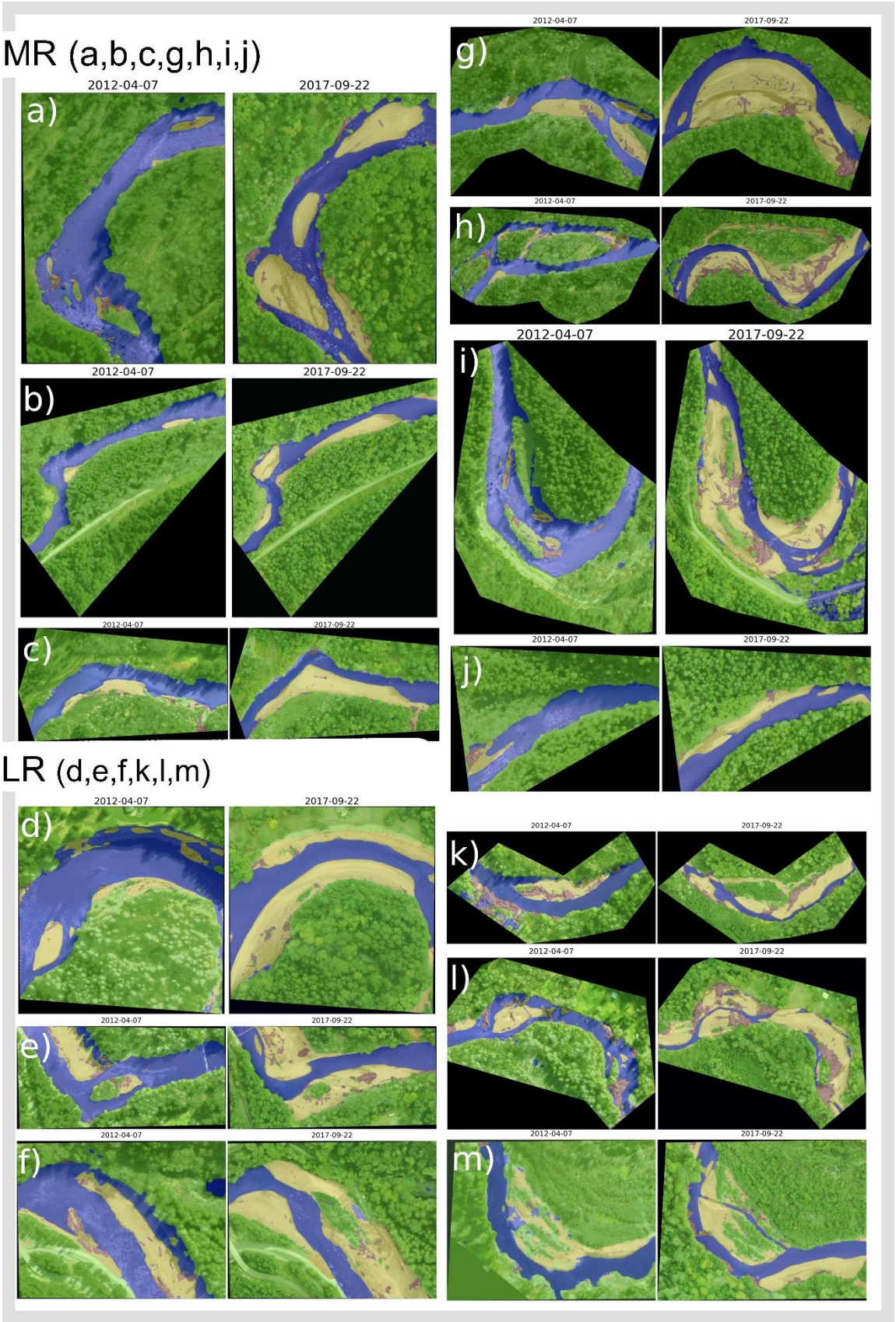
MR (a,b,c,g,h,i,j)
2012-04-07
2017-09-22
a)
b)
c)
g)
h)
i)
j)
LR (d,e,f,k,l,m)
d)
e)
f)
k)
l)
m)

Figure 6: Example model outputs for the first (2012-04-07) and last (2017-09-22) aerial survey from a selection of bars in the middle reach (MR) and lower reach (LR).

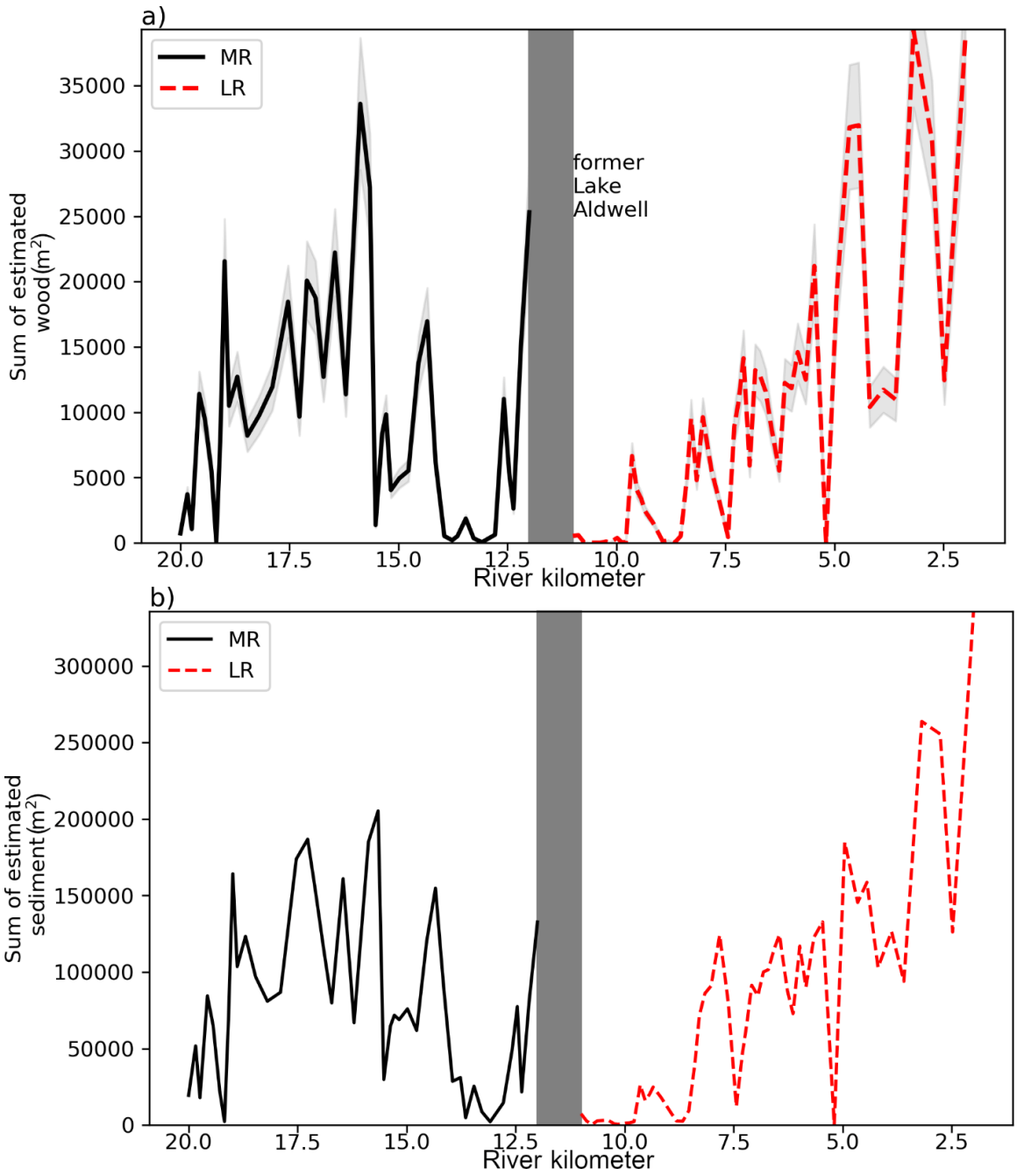

Figure 7: Total wood (a) and sediment (b) area as a function of downstream distance. Shading in a) is +/- 15%.

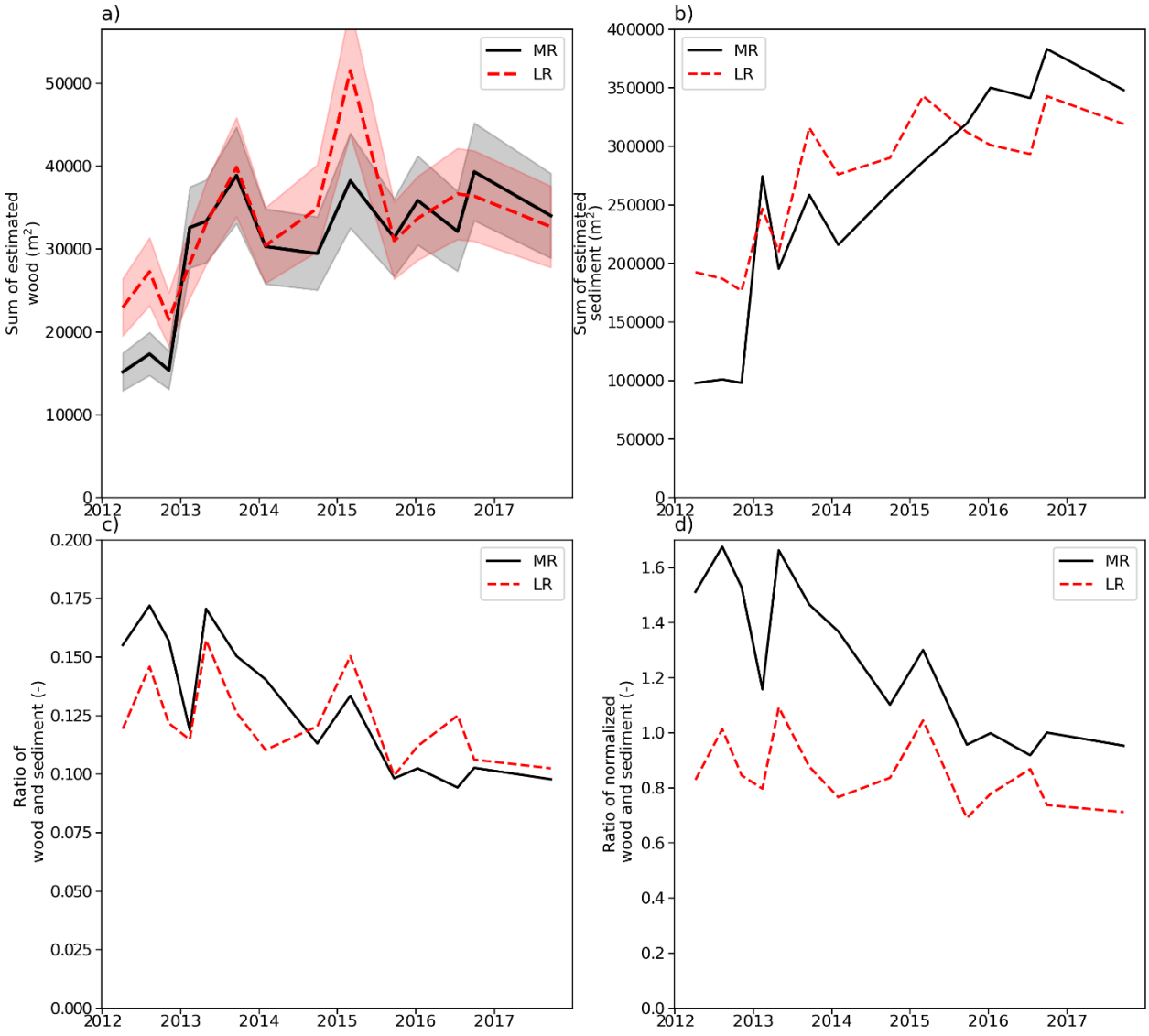

Figure 8: Time series of total a) wood and b) sediment areas, c) ratio of wood and sediment areas, and d) normalized ratio of wood and sediment, computed as the normalized sum of wood area divided by the normalized sum of sediment area. Shading in a) is +/- 15%.

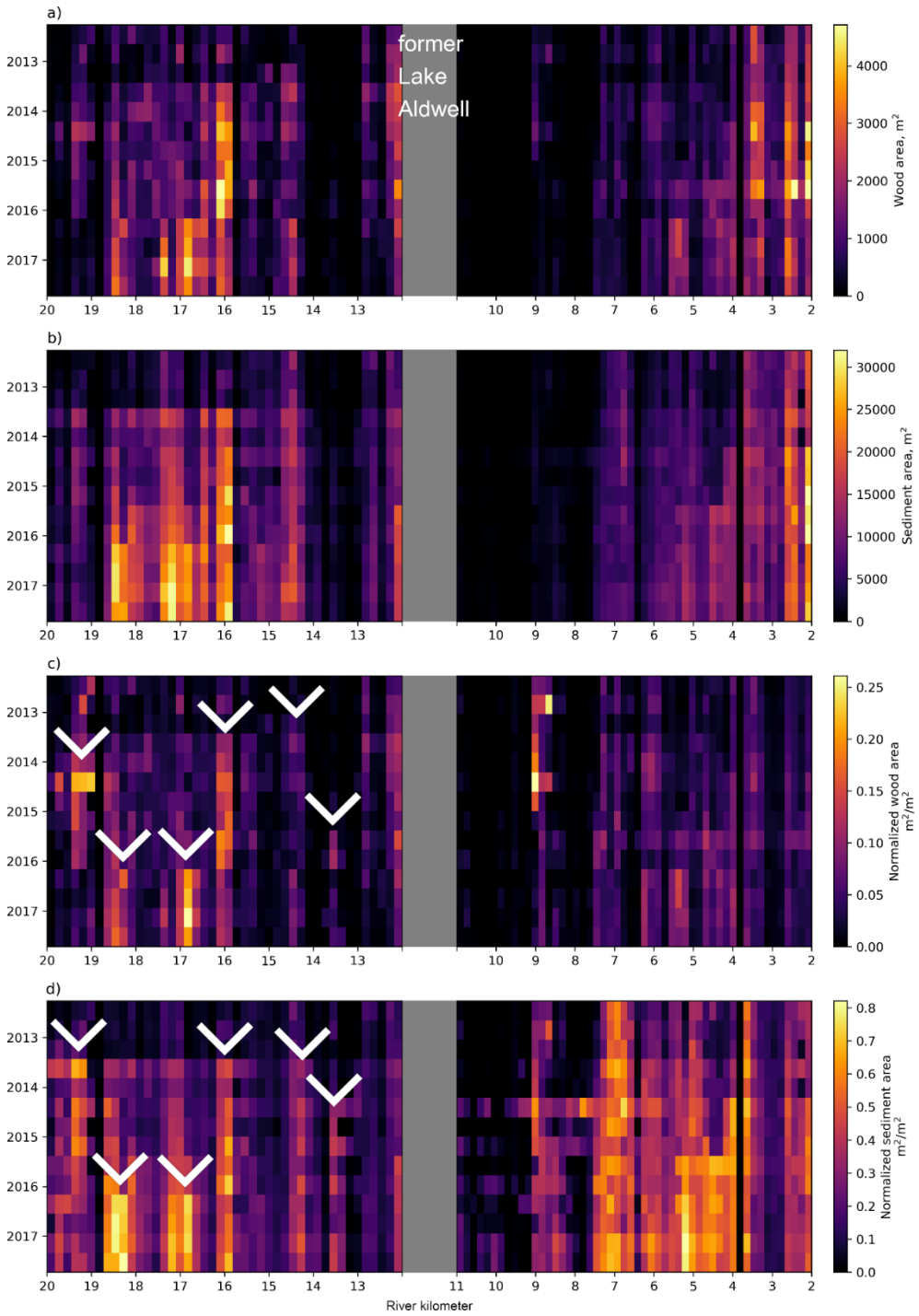

Figure 9: Wood and sediment deposit area (m^2) and normalized wood areal (i.e., wood concentrations) (m^2/m^2) in the middle reach (left column) and lower reach (right column). In each subplot, magnitudes are shown as a function of time (decreasing on the y axis) and distance downstream (decreasing on the x axis). Arrows in e) and g) refer to specific localized events discussed in the accompanying text.

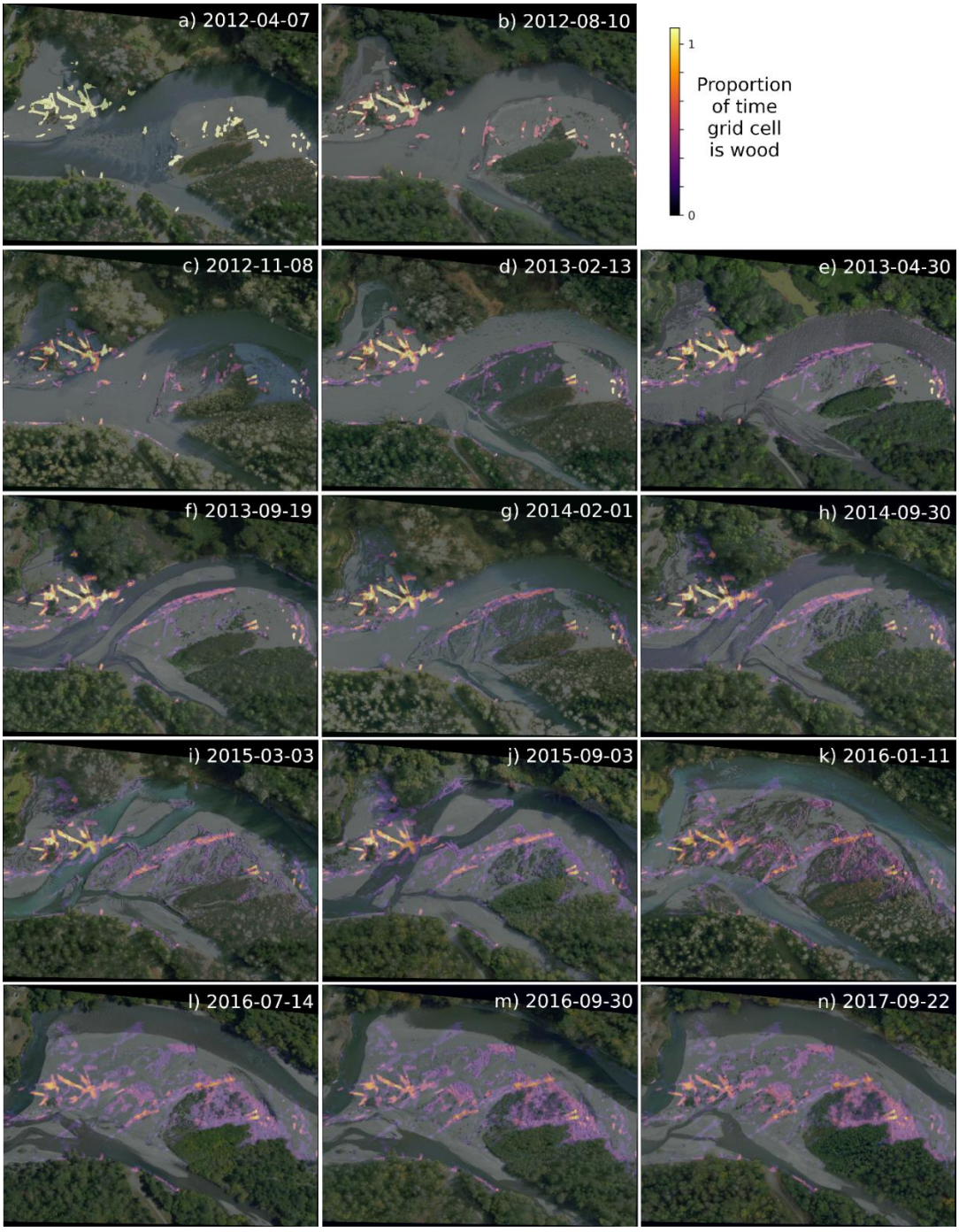

Figure 10: Example of large wood persistence near the middle of the lower reach where there was a modest amount of pre-existing wood. Each panel shows an orthoimage at a different time in the 14-point time series. The brightness of the superimposed persistence map is proportional to the proportion of cumulative time wood has been present at that location.

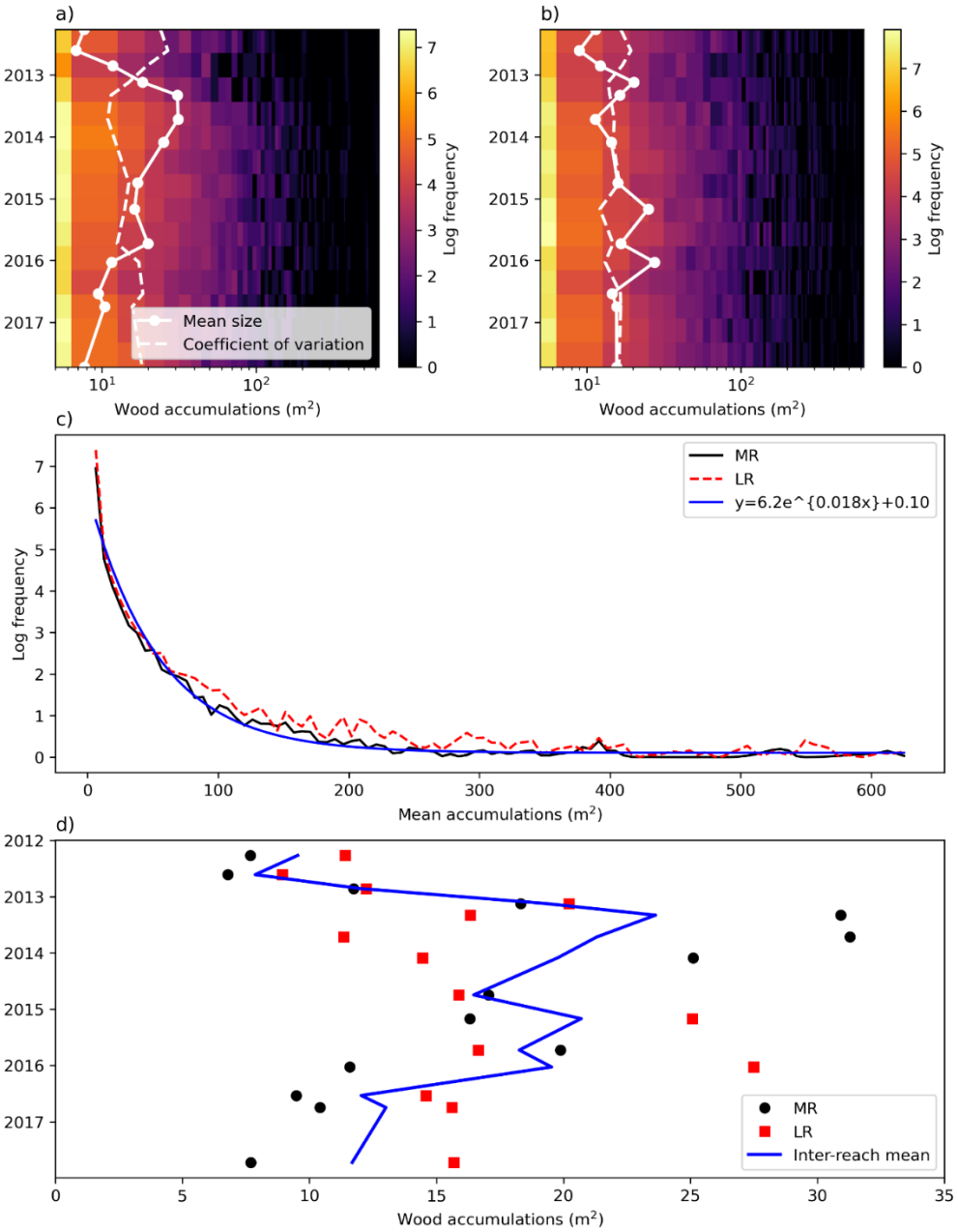

Figure 11: Time-varying wood size-distributions in the middle reach (MR; a) and lower reach (LR; b). The time series of mean wood piece/pile size and coefficient of variation of wood sizes are also shown. c) The time-averaged wood size-distribution in both reaches, conforming to an exponential distribution model fit to the data obtained using optimization methods. d) Time series of mean wood piece/pile size, and the inter-reach mean, which initially increased until 2014/2015, then decreased.

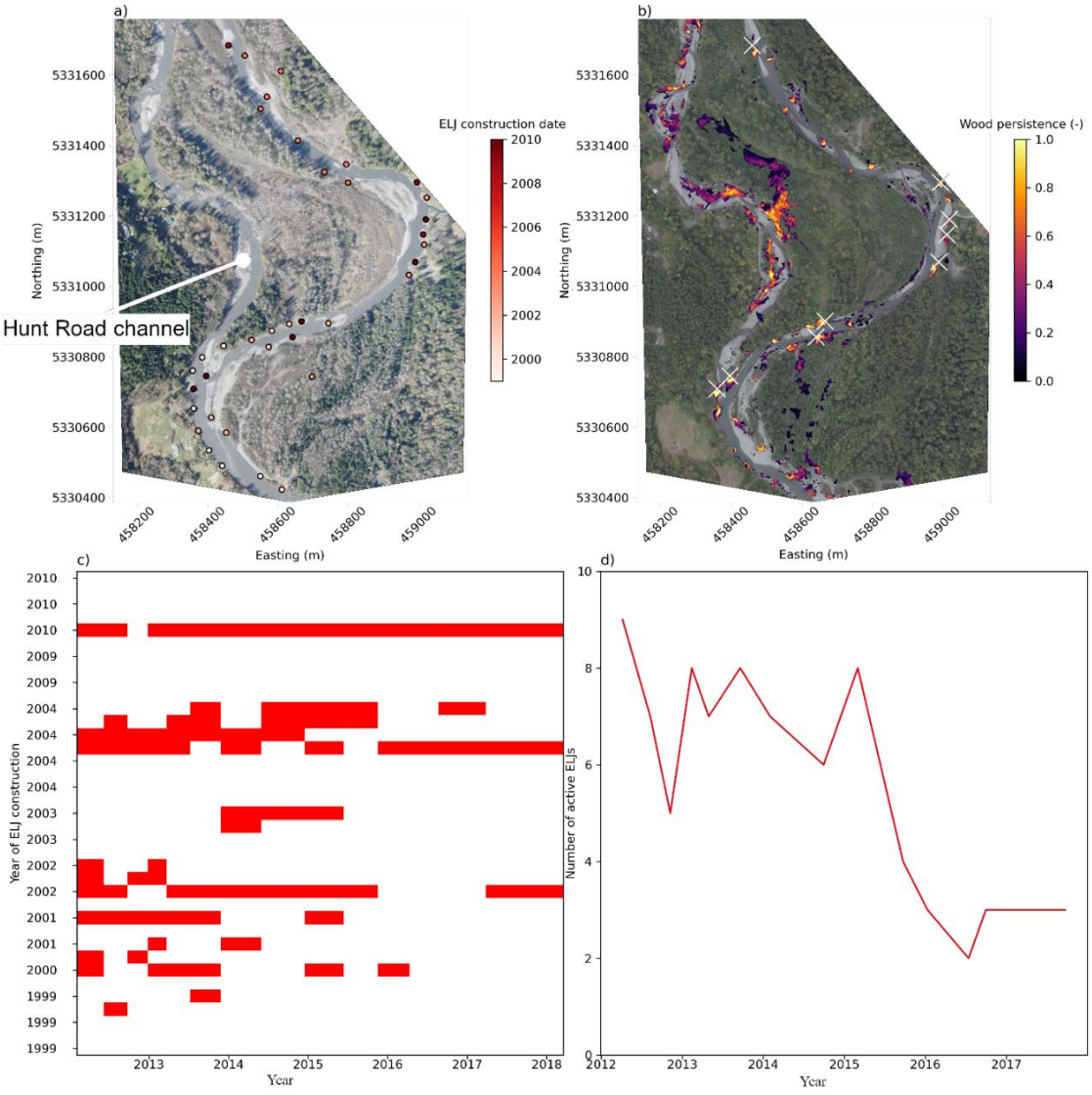

Figure 12: a) Locations of Engineered Log Jams (ELJs), colored by their date of construction (no new ELJs were constructed between 2010 and the end of the present study, September 2017.) Background image is from 2012-04-07. The river flows to the north, and the Hunt Road channel, which avulsed prior to this study, is indicated. b) The persistence of wood (the sum of wood pixels across all surveys) overlying the 2017-09-22 image, and with the post-2009 ELJ locations as white crosses. Note that the 2017-09-22 imagery in b) has had a gamma correction applied (with an exponent of 2.2) to enhance the brightness for better visibility. c) The presence (red bar) and absence (absence of red bar) at each ELJ (y axis), ordered by date of ELJ construction, and survey time (x axis). d) The number of active ELJs over time. Active ELJs are those with wood accumulations within 5m at time of survey.

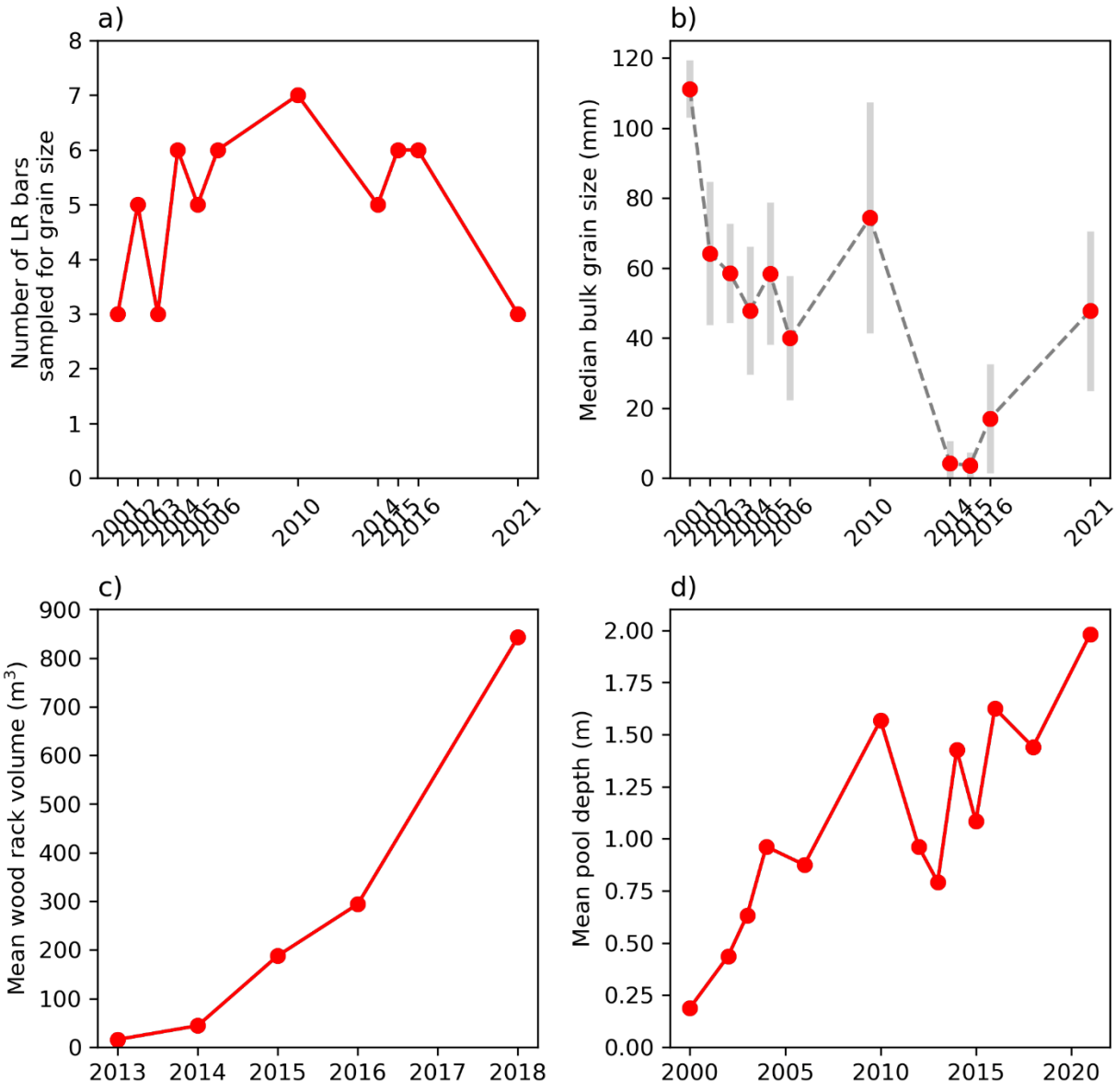

Figure 13: Time series measurements of lower reach bar grain size, wood rack volumes, and pool depths. a) number of bars sampled for grain size; b) Median grain size of lower reach alluvial bars (gray bars indicate +/- 1 standard deviation); c) Mean wood rack volume; and d) Mean pool depth.

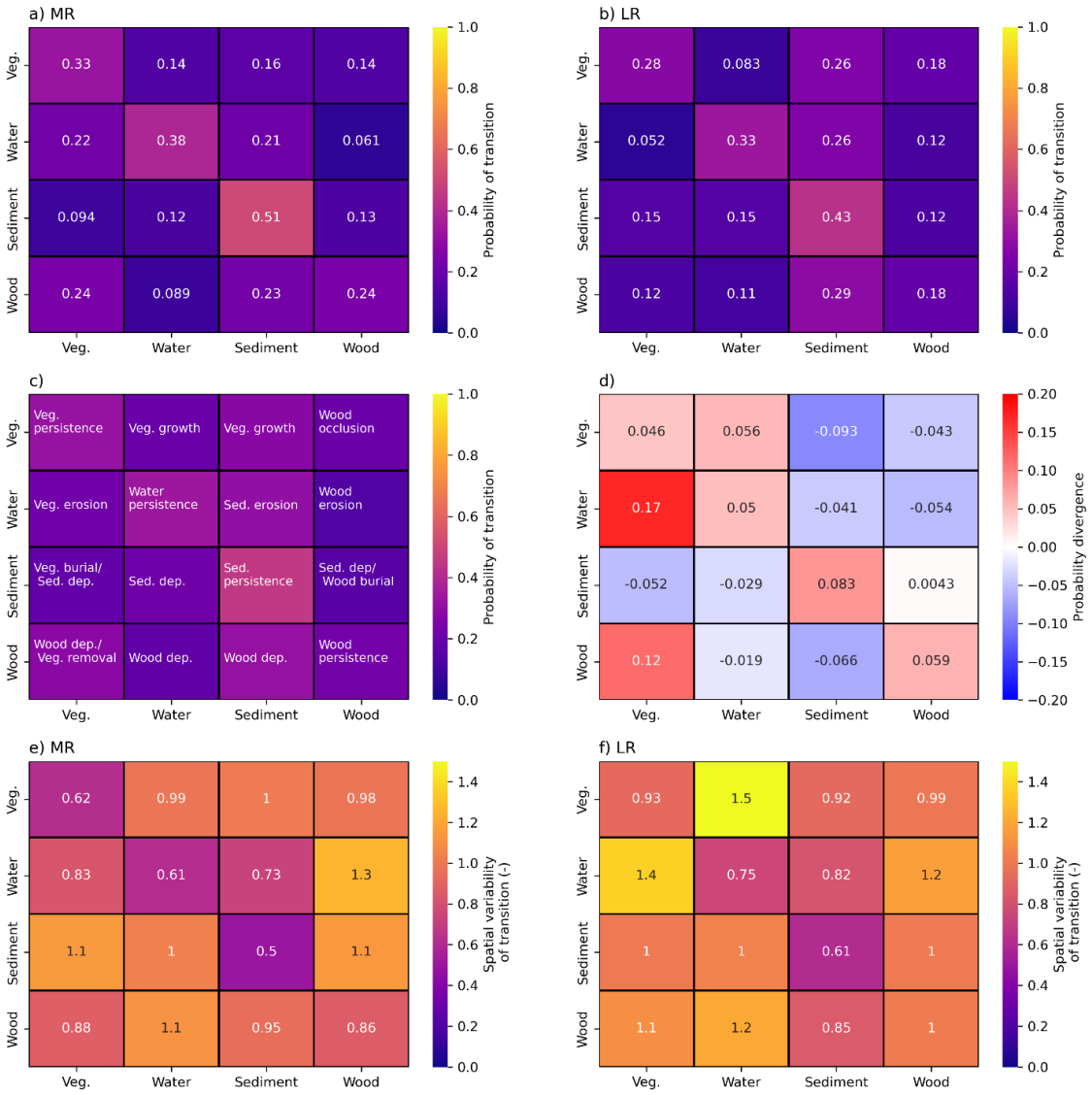

Figure 14: Transition probability matrices for the a) middle reach (MR) and b) lower reach (LR), based on an analysis of all 14 four-class (vegetation, water, sediment, wood) label maps. c) A schematic of the proposed 16 processes quantified by a transition matrix. Note that wood burial could alternatively or additionally be wood erosion. d) Divergence in probabilities between reaches, computed as MR minus LR, therefore positive numbers mean the process is more prevalent in the MR, and negative numbers indicate a process more prevalent in the LR. e) Coefficient of variation of TPMs computed over all subreaches of the MR and f) LR. The coefficient of variation is computed per cell as the standard deviation in transition probabilities divided by the mean transition probabilities. Large values therefore quantify highly spatially episodic (fluctuating) processes, whereas small values indicate spatial consistency.

Table 1: Summary of studies employing aerial remote sensing using visible band imagery only for large wood detection and quantification in rivers and river deltas. Many quantities have been estimated due to a lack of reporting of the dimensions of regions mapped, image pixel size, and other important details. See also Table 1 in Sendrowski and Wohl (2021), which lists other studies utilizing elevation-based and hyper-spectral imagery methods.

Study	Data source	Site	Mapped active channel (ha)	Number of surveys (total time)	Wood detection methods	Mapped units	Pixel horizontal footprint (m)
Marcus et al. (2002)	Fixed wing plane aerial nadir imagery (estimated)	Yellowstone, USA	~ 100 ha	Not clear. Several surveys on several rivers	Semi-automated (details lacking)	Large wood	Not reported, estimated < 1 m
Haschenburger and Rice (2004)	Fixed wing plane aerial nadir imagery	Carnation Creek, BC, Canada	~63 ha	One (details lacking)	Manual	Large wood	Not reported, estimated < 1 m
Smikrud and Prakash (2006)	Fixed wing plane aerial nadir imagery	Unuk River, AK, USA	32 ha	Two (2003 – 2004)	Semi-automated supervised classification	Large wood	0.8 m
Lassettre et al. (2008)	Aerial imagery	Ain River, France	~800 ha	Several (1945 to 2000)	Manual	Large wood	Not reported, estimated < 1 m
Ortega-Terol et al. (2014)	Aerial imagery	Jucar River, Spain	~ 2640 ha	One	Manual, semi-automated supervised classification	Large wood	0.25 m
Atha (2014)	Satellite	Queets River, WA, USA	~ 730 ha	One (composite of public satellite imagery)	Manual	Large wood	Not reported, estimated < 10 m
Ulloa et al. (2015)	Google Earth imagery, aerial imagery, and satellite image	Blanco River, Chile	~ 102 ha	Three (2005, 2009, 2012.)	Manual and semi-automated supervised classification	Large wood	0.5 – 2.4 m
Taminga et al. (2015)	Orthoimagery from small UAV (quadcopter)	Elbow River, Alberta, Canada	30 ha	One (Sept. 2012)	Manual	Large wood	0.05 m

Boivin et al. (2015)	Satellite and aerial imagery	St. Jean River, Quebec, Canada	~ 500 ha	Numerous (1963 – 2013)	Manual	Large wood	0.63 – 15 m
Kramer et al. (2017)	Satellite and aerial imagery	Slave River, NWT, Canada	4 sample locations in an estimated 6489 ha region	59 (1983 – 2014)	Manual and semi-automated supervised classification	Large wood	Not reported, estimated < 10 m
Sanhueza et al.(2019)	Orthoimagery from small UAV (quadcopter)	Blanco River, Chile	1.2 ha	One (Mar-Apr 2016)	Manual	Large wood	0.016 m
Tsunetaka et al. (2021)	Orthoimagery from small UAV (quadcopter)	Otoishi River, Kyushu, Japan	35.2 ha	Two (2018 – 2019)	Manual	Large wood	0.03 – 0.05 m
Sendrowski et al. (2023)	Satellites (GeoEye, Quickbird, and WorldView)	Mackenzie River Delta, AK, USA	35,000 ha	Not reported (combined 2009 – 2021)	Manual delineation to train fully automated deep learning model. Manual post-processing.	Large wood	0.3 – 0.65 m
Iroumé et al. (2023)	Orthoimagery from small UAV (quadcopter)	Blanco Este River, Chile	10.9 ha	17 (2017-2020)	Manual	Large wood	0.02 m
This study	Orthoimagery from fixed wing airplane	Elwha River, WA, USA	246 ha	14 (2012 – 2017)	Manual and semi-automated delineation to train fully automated deep learning model	Large wood, sediment, water, vegetation	0.125 m

	Overall accuracy	Frequency weighted Intersection over Union	Mean Intersection over Union	Matthews Correlation Coefficient
Wood (binary)	0.98	0.96	0.67	0.49
Sediment (binary)	0.95	0.92	0.79	0.73
Water (binary)	0.99	0.98	0.84	0.28
Other (binary)	0.99	0.97	0.88	0.65
Multiclass (wood, sediment, water, vegetation)	0.95	0.91	0.63	0.69

Table 2: Image semantic segmentation model accuracy statistics. Each row represents a different trained model, and each numeric column summarizes a different accuracy statistic.

	F1 score	Recall	Precision
Vegetation	0.98	0.99	0.99
Water	0.90	0.91	0.92
Sediment	0.72	0.74	0.75
Wood	0.60	0.81	0.53

Table 3: Multiclass segmentation model accuracy statistics. Each row represents a different class, and each numeric column summarizes a different accuracy statistic.

	Correlation coefficient
Wood abundance (time), MR and LR	0.78
Sediment abundance (time), MR and LR	0.89
Wood and sediment abundance (time), MR	0.86
Wood and sediment abundance (time), LR	0.77
Wood and sediment abundance (space), MR	0.88
Wood and sediment abundance (space), LR	0.92

Table 4: Correlations between distributions of wood and sediment in the middle reach (MR) and lower reach (LR).